J Membrane Biol (2010) 234:75–112
DOI 10.1007/s00232-010-9228-7

Reassessment of Models of Facilitated Transport and Cotransport

Richard J. Naftalin

Received: 18 November 2009 / Accepted: 8 January 2010 / Published online: 5 March 2010

Abstract Most membrane transport models are determinate, requiring the transported ligand(s) to bind initially to a vacant site, which undergoes translation and releases ligand to the alternate side. The carrier reverts to its initial position to complete the net transport cycle. Ligand affinity may change during translation, but this must be compensated by an equivalent energy change(s) within the transport cycle. However, any asymmetric cyclic equilibrium deduced on this basis is thermodynamically fallacious. Determinate cotransport models imply lossless stoichiometric relationships between the complexed cotransported ligands. Independent ligand leakage apart from the mobile cotransport complex must occur outside the canonical cotransport pathway. In contrast, stochastic transport models assume independent ligand diffusion through a variably occluded channel(s) containing binding sites where ligands may undergo bimolecular exchanges. Energy dissipation is intrinsic to all stochastic transport models and occurs within the primary transport pathway. Frictional interactions within a shared path generate flow coupling between ligands. The primary driving forces causing transmembrane ligand flows are their electrochemical potential differences between the external solutions. Demonstrations that ligand exchanges in CLC and neurotransmitter transporters can be multimodal, encompassing both "channel"-like high and "transporter"-like lower conductance states and have independently regulated import and export exchange fluxes are major challenges to determinate models but are explicable by transient widening of a close-encounter region within the channel, leading to decreased coupling and enhanced efflux.

R. J. Naftalin (✉)
Department of Physiology, King's College London, Waterloo Campus, Franklin–Wilkins Building, London SE1 9HN, UK
e-mail: richard.naftalin@kcl.ac.uk

Keywords Glucose transport · Asymmetric carrier · Thermodynamics · Symport · Antiport sodium · Glucose · Potassium · Chloride · Serotonin · Dopamine · GLUT · SGLT · SERT · DAT · CLC

Some Reasons Why the Theoretical Basis for the Conventional Models of Passive Downhill Facilitated Carrier Transport and Cotransport Is Deficient

Glucose transport via glucose transporter proteins (GLUTs, SLCA2) (Joost et al. 2002) across cell membranes is an instructive example of an asymmetric transport process of a single ligand. Models describing this process embody many of the underlying principles discussed in this review. Another major type of asymmetric transport is exemplified by cotransport via the sodium–glucose symport (SGLT, SLC5A1). This serves as a basic guide to the principles underlying other, more complex coupled ligand transport processes observed with neurotransmitter sodium symporters for noradrenaline, dopamine and serotonin (NISS, SLC6A2–4, respectively) and for anion:proton exchanges in CLC transporters. These will be discussed in the context both of their 3D structures and bimodal "channel–carrier" transitions of their exchange transport modes.

The Asymmetric Passive Alternating Transporter Model

What Is Asymmetric Transport?

Net glucose transport rates, as observed in human erythrocytes, are normally measured from a solution containing glucose (*cis*) into the nominally glucose-free solution on

the other side of the cell membrane (*trans*). The glucose concentration at which the transport rate is half-maximal in the *cis* solution, the K_m, is an inverse measure of the apparent affinity of the transported ligand for the adjacent binding site. This apparent affinity can differ from the true binding affinity, K_D, as transport rates are compounded from rate constants pertaining to both binding and transport, whereas binding relates only to association and dissociation rates of ligand from the site.

At 24°C the erythrocyte glucose transporter GLUT1 has approximately a 10-fold lower affinity for D-glucose ($K_m \approx$ 10–15 mM) at the inside face for net export than on the outside (K_m = 1–2 mM) for net import of glucose (*zero*-trans *net flux*). At 4°C the affinities are higher and the asymmetry is larger than at 24°C and 37°C (Brahm 1983; Naftalin and Arain 1999) (see Fig. 2c below, Table 1). At equilibrium,

$$\mu^{out}_{Glc} - \mu^{in}_{Glc} = 0 \tag{1}$$

Kinetics of Glucose Uniport

The formal description of asymmetric carrier systems was adapted from the symmetric mobile carrier model. The glucose carrier has conventionally been described using a four-node cyclic network (Fig. 1a) (Baker and Widdas 1973; Geck 1971; Ginsburg and Stein 1975; Hankin et al. 1972; Lieb and Stein 1974; Lowe and Walmsley 1986; Miller 1971; Regen and Morgan 1964; Regen and Tarpley 1974; Stein 1989). Glucose in the external solution first binds to the externally facing high-affinity vacant carrier site (node 1), forming a high-affinity outward-facing glucose–carrier complex (K^{out}_D = 1 mM) (node 2). The external glucose–carrier complex then translates to the inside (node 3) and in the process is transformed to a lower-affinity complex (K^{out}_D = 10 mM). After glucose release into the cytoplasm, the low-affinity inward-facing vacant site (node 3) completes the net transport cycle by returning to the external phase and, in so doing, regenerates the higher-affinity outward-facing vacant site (node 1). As glucose transport is passive, the entire transport scheme is reversible.

Detailed balance is conserved in the cyclic carrier model by making the product of all the clockwise rates equal to the product of all anticlockwise rates for the four-node cycle (Klein 1955) (Fig. 1a).

$$k_{12} \cdot k_{23} \cdot k_{34} \cdot k_{41} = k_{21} \cdot k_{14} \cdot k_{43} \cdot k_{32} \tag{2}$$

and for the three-node cycle (Fig. 1b)

$$k_{12} \cdot k_{23} \cdot k_{31} = k_{21} \cdot k_{13} \cdot k_{32} \tag{3}$$

Thus, since $K^{out}_D = k_{21}/k_{12}$ and $K^{in}_D = k_{34}/k_{43}$ and assuming the energy compensation step resides solely within movements of the vacant carrier, then

$$k_{23} = k_{32} \tag{4}$$

According to Eq. 2, differing dissociation constants at the inside K^{in}_D and outside K^{out}_D sites are permissible, providing the ratio k_{14}/k_{41} maintains detailed balance.

Combining Eqs. 2 and 3 gives

$$\frac{K^{out}_D}{K^{in}_D} \cdot \frac{k_{14}}{k_{41}} = 1, \text{ or } \frac{K^{out}_D}{K^{in}_D} = \frac{k_{41}}{k_{14}} \tag{5}$$

The Law of Mass Action and Carrier Energy Distribution

$k_{21}/k_{12} = K^{out}_D$ and $k_{34}/k_{43} = K^{in}_D$, and C^i and GC^i are the proportions of vacant and liganded carriers in phase^i, respectively. When the law of mass action is applied to the four-node asymmetric glucose carrier, $C^i_{carrier}$, with equal concentrations of glucose, Glc is present in the solutions on either side of the membrane (Fig. 1a):

$$\begin{aligned} \left[C^{out}_{carrier}\right] \cdot \left[Glc^{out}\right] \cdot k_{12} &= \left[GC^{out}\right] \cdot k_{21} \quad \text{and} \\ \left[C^{in}_{carrier}\right] \cdot \left[Glc^{in}\right] \cdot k_{43} &= \left[GC^{out}\right] \cdot k_{34} \end{aligned} \tag{6}$$

and

$$\begin{aligned} \left[C^{out}_{carrier}\right] \cdot \left[Glc^{out}\right] &\leftrightarrow \left[GC^{out}\right] \cdot K^{out}_D \quad \text{and} \\ \left[C^{in}_{carrier}\right] \cdot \left[Glc^{in}\right] &\leftrightarrow \left[GC^{in}\right] \cdot K^{in}_D \end{aligned} \tag{7}$$

Table 1 Simulated operational Michaelis–Menten parameters of observed 3-OMG fluxes at 4°C obtained with the asymmetric two fixed site model

Condition	K_m (mM) (observed)	V_m (mmol l^{-1} min^{-1}) (observed)	V_m/K_m (observed)	K_m (mM)	V_m (s^{-1})	V_m/K_m
Zero *trans* entry	0.38	0.18	0.47	0.4	0.12	0.30
Zero *trans* exit	4.35	1.62	0.37	7.3	2.10	0.29
Equilibrium exchange	22.62	9.17	0.41	14.7	10.0	0.68
Infinite *trans* entry	1.57	5.62	3.58	1.38	8.8	6.37

Parameters for two-fixed site simulation to fit the flux parameters obtained by Cloherty et al. (1996) of 3-*O*-methyl-D-glucoside fluxes in human erythrocytes at 4°C

K^{out}_D = 0.5 mM, K^{in}_D = 12 mM, $k_{01} = 10\ s^{-1}$, $k_{43} = 12\ s^{-1}$, $k_{23} = k_{32} = 0.025\ s^{-1}$, $k_{exchange} = 10\ s^{-1}$

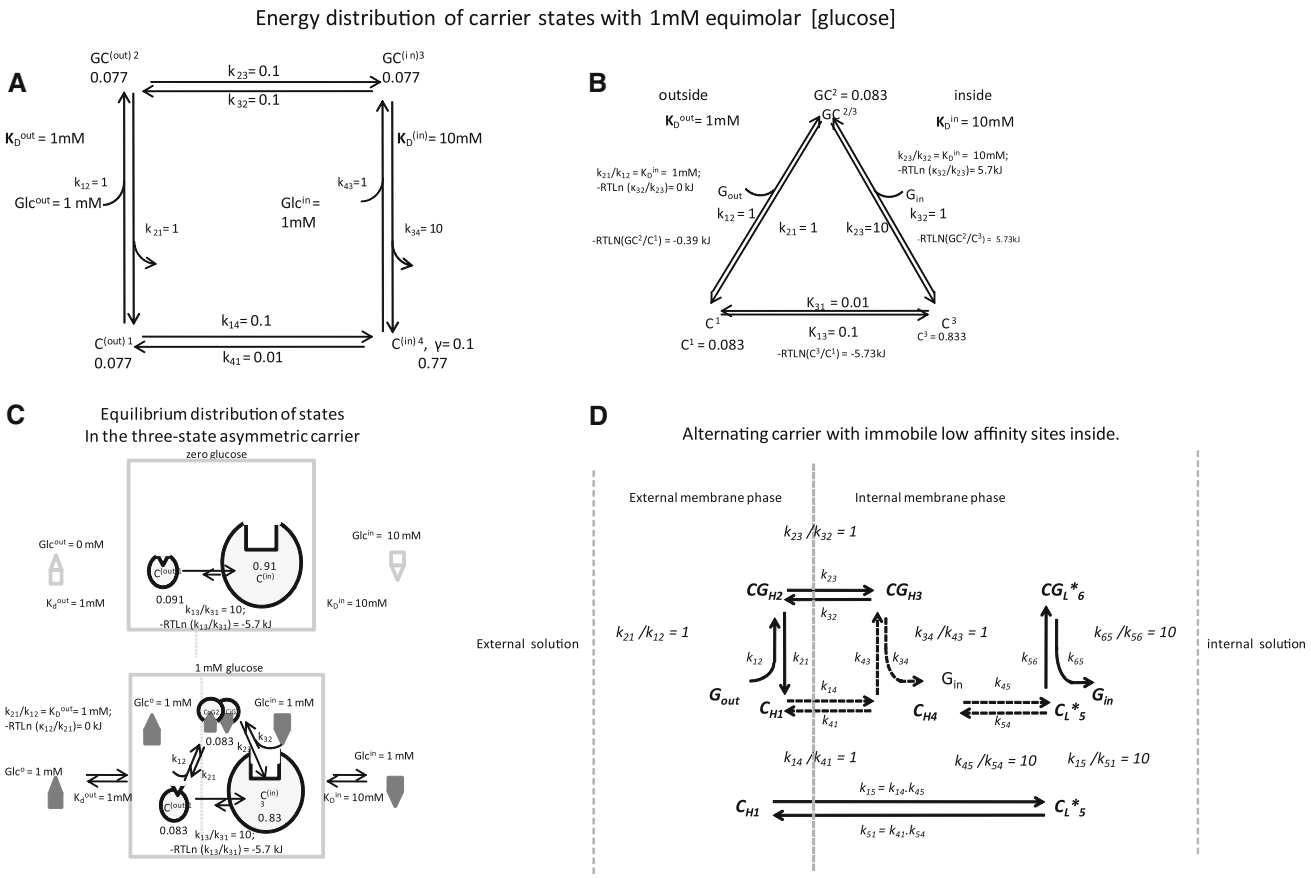

Fig. 1 **a** The proportions of each carrier state for the conventional four-state alternating carrier—C_1, GC_2, GC_3 and C_4—are shown with equimolar glucose concentrations in the external solutions of 1 mM with the asymmetric affinities and rates as shown in **c**. **b** The proportions of each carrier state C_1, GC_2 and C_3 are shown with equimolar glucose concentrations in the external solutions of 1 mM with the asymmetric affinities and rates shown in **c**. **c** An illustration of the relative proportions of carrier form predicted by the three-state asymmetric mobile carrier assuming the inside site has a $K_D = 10$ mM, the outside site has a $K_D = 1$ mM and both external solutions contain 1 mM glucose. All rate constants are as shown in **a** and **b** for the asymmetric carrier. The relative sizes of the carrier forms $1 = 2 = 0.083$ and $3 = 0.83$ illustrate the relative proportions of each carrier state, and the energy differences between these states are shown beside the *connecting arrows* between the states. **d** A deconstructed version of the single asymmetric alternating-site carrier model showing the hidden steps (*broken arrows*) obscured by kinetic lumping of the phase transfer reaction of mobile vacant carrier C_H and CG_H across the membrane and the unimolecular isomerization reaction of high-affinity vacant mobile carrier C_H to low-affinity immobile carrier C^*_L in the internal membrane phase

As the transmembrane flux rates of the carrier complex are assumed to be equal ($k_{23} = k_{32}$, Eq. 4) at equilibrium, the "concentrations" of carrier–ligand complex, GC^i, are also equal. Hence, from Eqs. 6 and 7,

$$\frac{C^{out}_{carrier}}{K^{out}_D} = \frac{C^{in}_{carrier}}{K^{in}_D} \quad \text{or} \quad \frac{C^{in}_{carrier}}{C^{out}_{carrier}} = \frac{K^{in}_D}{K^{out}_D} \tag{8}$$

The relationships in Eq. 8 show that if transporter affinity for glucose is 10-fold lower on the inside than the outside, i.e., $\frac{K^{in}_D}{K^{out}_D} = 10$, equal rates of the glucose–carrier complex (GC) flow in opposite directions at equilibrium with equal glucose concentrations present in the internal and external bathing solutions, requiring that the vacant carrier on the inside, C^{in}, be 10-fold higher than C^{out} (Fig. 1c).

The four-node cyclic carrier scheme can be simplified to a three-node cycle (Stein 1989), in which the external and internal faces (nodes 2 and 3) of the glucose carrier are condensed to a single node and assumed to be centrally positioned (Fig. 1b). However, compensation for ligand binding asymmetry can be distributed in any proportion between the asymmetries of the transmembrane flux rates of either the vacant or liganded carrier without changing the underlying assumptions (Naftalin 2008a).

Conservation of the Haldane Relationships with Asymmetric Transport

It may be deduced from Eqs. 2–4 that the Haldane relationships for the operational flux parameters K_m and V_m that the ratios V_m/K_m for inflow and outflow are equal (Stein 1989) thus:

$$V_m^{import}/K_m^{import} = V_m^{export}/K_m^{export}. \quad (9)$$

Although this simple relationship is a necessary corollary of the cyclic carrier model, it has often been experimentally observed that V_m and K_m for import and export do not conform to the symmetry prediction of the Haldane relationships; and from this, it is deduced that the cyclic carrier model is an inadequate description of glucose transport (Baker and Naftalin 1979; Cloherty et al. 1996). However, although experiments are necessary for discovery, they are imprecise and therefore always subject to uncertainty. Determinate models for asymmetric transport can only be falsified unequivocally by logical demonstration that their thermodynamic basis is unsound.

Thermodynamic Implications of Cyclic Asymmetric Carrier Models

If the alternating carrier has symmetric affinities and there are equal activities of transported ligand in the solutions on either side, bound ligand passes between the two sides of the transporter without any affinity or consequent energy changes. No energy change occurs either when the vacant carrier returns via the short transmembrane branch to complete the net transport cycle (Fig. 1b). Thus, the symmetric carrier system is in both material and energy equilibrium.

However, when the alternating carrier is asymmetric, loss of ligand complexed with the higher-affinity site from the outside, followed by its reappearance on the inside, bound to a lower-affinity site, implies a dual process involving both spatial translation between different membrane phases and energy transformation resulting from changes in Gibbs' free energy (ΔG_{Glc}) due to the changes in ligand affinity at the binding site.

The gain in kinetic energy during transit of bound glucose via the pathway $1 \rightarrow 2 \rightarrow 3$ from high to low affinity (Figs. 1b, 2e, panel a) or $1 \rightarrow 2 \rightarrow 3 \rightarrow 4$ (Fig. 1a) with a consequent higher dissociation rate from the inside site should result in a higher ligand concentration in the cytoplasmic solution adjacent to the low-affinity site at equilibrium.

$$\Delta G_{Glc} = -RTLn\frac{K_D^{out}}{K_D^{in}} = -RTLn\frac{1}{10} = 5.74\,kJ \quad (10)$$

However, the detailed balance constraint Eqs. 2–5 require

$$\frac{\text{vacant carrier outflow rate, } k_{31}}{\text{vacant carrier inflow rate, } k_{13}} = \frac{K_D^{out}}{K_D^{in}} \quad (11)$$

The asymmetric rates of vacant carrier movement deplete free carrier from the external surface and augment the proportion of vacant carrier facing inward, thereby retarding the maximal rate of glucose entry and accelerating glucose exit (Fig. 1c). Thus, when ligand concentrations are equal in the internal and external bathing solutions, there are equal unidirectional movements of vacant carrier so that net flow is zero (Fig. 1b).

$$C_{carrier}^{out} \cdot k_{13} = C_{carrier}^{in} \cdot k_{31} \quad (12)$$

In addition to zero net flow of matter, the asymmetric carrier model requires that energy released by downhill flow of vacant carrier via the shorter branch of the cycle $3 \rightarrow 1$ (Fig. 1b, c) will compensate for the asymmetric energy flows via the longer branch of the cycle, so there is a zero net sum of energy flow around the transport cycle.

$$\Delta G_{carrier} = -RTLn\frac{C_{carrier}^{(in)}}{C_{carrier}^{(out)}} = -RTLn\frac{10}{1} = -5.74\,kJ \quad (13)$$

However, even in the absence of ligand, the asymmetric alternating access carrier theory requires that the vacant carrier have an asymmetric distribution between the two sides of the transporter generated by the energy from asymmetric rates of free carrier equilibration (Fig. 1c). Application of the van't Hoff equation (Kondepudi and Prigogine 1998) gives

$$\Delta G_{carrier} = -RTLn\frac{k_{13}}{k_{31}} = -RTLn\frac{10}{1} = -5.74\,kJ \quad (14)$$

As there is no exogenous source for the energy generating the asymmetric distribution of vacant carrier, it must arise spontaneously. The absence of any exogenous energy source is indicated by the broken arrow in Fig. 2e (panel a). The difference in energy between the tightly bound ligand at the external site and the more loosely bound ligand at the internal site is apparently compensated by the higher concentration of vacant carrier inside than outside. However, the energy needed to generate this asymmetric carrier distribution comes only from the assigned flux ratio of free carrier, needed to enforce the detailed balance constraint, not from any exogenous source. This point is well illustrated by Ussing's (1949) flux ratio equation, in which active transport of Na^+ across isolated frog skin is characterized by asymmetric rate constants. Consequently, the passive processes which characterize glucose equilibration via facilitating transporters require the ratio of bidirectional transport rates.

$$\frac{k_{13}}{k_{31}} = 1$$

Thus, the assumption of asymmetric rates of vacant carrier movement simply shifts the overt thermodynamic fallacy of an equilibrium state obtaining with unequal external ligand concentrations to a covert fallacy, where there is unequal vacant carrier distribution at equilibrium buried within the membrane.

The Phase Equilibrium Fallacy

It has been argued that the alternating-site transporter can be asymmetrically distributed either because of differences in the standard free energy, μ_c^0 (Lapointe et al. 2009), or because of activity coefficients, γ_c (Naftalin 2008a), of the vacant carrier isoforms, $C^i_{carrier}$, between the opposing membrane sides or phases. Thus, if $C^{in}_{carrier} > C^{out}_{carrier}$, then either $\mu^{0\ in}_{carrier} < \mu^{0\ out}_{carrier}$ or $\gamma^{in}_{carrier} < \gamma^{out}_{carrier}$. Thus, at equilibrium the Gibbs free energy difference, $\Delta G_{carrier}$, of the vacant carrier distribution

$$\Delta G_{carrier} = \Delta\mu^0_{carrier} + RTLn\left(\frac{C^{out}_{carrier}}{C^{in}_{carrier}}\right) = 0 \tag{15}$$

$$\text{hence if } \Delta G_{carrier} = 0 \text{ and } \Delta\mu^0_{carrier} = 5.74\,kJ = \frac{C^{out}_{carrier}}{C^{in}_{carrier}} = 0.1 \tag{16}$$

Alternatively, if the standard free energies are the same in both membrane phases but the activity coefficients are unequal so that

$$\frac{\gamma^{in}_{carrier}}{\gamma^{out}_{carrier}} = 0.1,$$

$$\text{then } \Delta G_{carrier} = RTLn\left(\frac{C^{out}_{carrier}\gamma^{out}_{carrier}}{C^{in}_{carrier}\gamma^{in}_{carrier}}\right) = 0 \text{ and } \frac{C^{in}_{carrier}}{C^{out}_{carrier}} = 10 \tag{17}$$

In both cases, at equilibrium, where $\Delta G_{carrier} = 0$, $\frac{C^{in}_{carrier}}{C^{out}_{carrier}} = 10$.

As the carrier partition coefficient between the inside and outside ($P_{in/out}$)

$$P_{in/out} = \frac{C^{in}_{carrier}}{C^{out}_{carrier}} \tag{18}$$

(Kondepudi and Prigogine 1998; Prausnitz et al. 1986), then from Eq. 15

$$\Delta\mu^{0\,out-in}_{carrier} = -RTLn\left(P_{in/out}\right) \tag{19}$$

$$\text{Thus, } \Delta G_{carrier} = RTLn\left(\frac{C^{out}_{carrier}}{C^{in}_{carrier}\cdot P_{in/out}}\right) = 0 \tag{20}$$

Since at equilibrium, as in Eq. 11, unidirectional vacant carrier flows, $k_{ij}\cdot c^i$, are equal, from Eqs. 12 and 18

$$k_{out-in}\cdot C^{out}_{carrier} = k_{in-out}\cdot C^{in}_{carrier}, \text{ and } \frac{C^{in}_{carrier}}{C^{out}_{carrier}} = \frac{k_{out-in}}{k_{in-out}} = P_{in/out} \tag{21}$$

Thus, to account for the asymmetric carrier distribution at equilibrium between the heterogeneous inner and outer membrane phases, where either the standard free energy (μ^0_c) or activity (γ_c) coefficient of vacant carrier differs between phases, the van't Hoff equation,

$\Delta G_{carrier} = RTLn\left(\frac{k_{out-in}}{k_{in-out}}\right)$, which is applicable only to a single phase (Kondepudi and Prigogine 1998) or to homogeneous membrane phases, requires a correction:

$$\Delta G_{carrier} = RTLn\left(\frac{k_{out-in}}{k_{in-out}\cdot P_{in/out}}\right) = 0, \text{ or } \Delta G_{carrier} = RTLn\left(\frac{k_{out-in}\cdot\gamma^{in}_{carrier}}{k_{in-out}\cdot\gamma^{out}_{carrier}}\right) = 0. \tag{22}$$

However, once these corrections are applied, neither the asymmetric flux ratios nor the vacant carrier distributions compensate for the energetic difference resulting from the asymmetric ligand affinities,

$$\text{if } K^{out}_D < K^{in}_D, \text{ then } \Delta G^{affinities}_{carrier} = RTLn\left(\frac{K^{out}_D}{K^{in}_D}\right) < 0$$

Since a passively acquired asymmetric distribution of vacant carrier at equilibrium generates no force, i.e., $\Delta G_{carrier} = 0$, no energy is available from the vacant carrier distribution to counterbalance any energy difference resulting from asymmetric ligand affinities, $\Delta G^{affinities}_{carrier} \neq 0$.

In a recent critique of these views (Lapointe et al. 2009), it is stated that the activities of mobile components on either side of the membrane do not have to be the same if the standard free energies differ. While this is the case, once the necessary correction has been applied to the van't Hoff equation, as shown above in Eq. 22, to convert the flux ratios of mobile ligands between heterogeneous phases to energetic flows, the asymmetric free carrier distribution between the inner and outer membrane phases no longer compensates for the asymmetric ligand binding asymmetries between the external aqueous solutions and their adjacent membrane sites.

A concrete example of a passive asymmetric distribution between heterogeneous phases is the distribution of an amphiphile, like benzoic acid, between benzene and water. At equilibrium no energy difference for benzoic acid exists between the solutions despite the large concentration asymmetry between the phases (Prausnitz et al. 1986).

The Asymmetric Carrier Violates Gibbs Phase Rule

A mobile component, C^i, has equal mobility in either direction between connected phases[j], and although this can be catalysed by transporters, the translation process involves only diffusion.

A chemical reaction involving molar free energy change cannot be a conditional determinant for ligand transition between phases[j], e.g., unimolecular isomerization $C_H \leftrightarrow C_L$. Were this so, then in contravention of the Gibbs phase

rule, C_H^{ex} and C_L^{in} could be absent from their alternate phases at equilibrium. However, the Gibbs phase rule requires equal chemical potentials at equilibrium of all mobile components, C_i in all connected phases[j]. To attain a chemical equilibrium between components C_i in different phases[j], C_H and/or C_L must cross the phase boundary prior to and independently of any chemical reaction occurring within either phase (Kondepudi and Prigogine 1998).

If C_H is mobile and C_L is immobile, the Gibbs phase rule requires that only the mobile component, C_H, equilibrates between the connected phases, so at equilibrium

$$\mu C_H^{out} = \mu C_H^{in} \tag{23}$$

In phase[in] the spontaneous chemical isomerization reaction, transforming C_H^{in} to C_L^{in}, where the standard free energy of the product C_L and reactant C_H differs, reaches equilibrium when

$$\mu C_H^{in} = \mu C_L^{in} \tag{24}$$

Thus, at equilibrium, the concentration of C_L^{in} differs from that of C_H^{in} and C_H^{ex}. However, the chemical potentials of C_H remain equal in both phase[out] and phase[in], independent of any chemical reaction transforming C_H^{in} to C_L^{in}.

Despite its alleged mobility, the high- and low-affinity carrier isomers are assigned only to single alternate phases in the conventionally asymmetric carrier model (Fig. 1a). Deconstructing the asymmetric transition k_{14}/k_{41} (Fig. 1a) into its constituent steps (Fig. 1d) demonstrates that the vacant carrier transition consists of a symmetric phase transition in sequence with an isomerization reaction. This results in an apparent asymmetric distribution of high- and low-affinity vacant carrier states in the inner membrane phase. However, elision of the two-stage process into a one-stage rate process hides the need for phase equilibration of the mobile component C_H between the inner and outer membrane phases. It also obscures the failure of the model system to account for asymmetric glucose transport since the low-affinity form is immobile and isolated from the transport cycle, so the only way that the sugar can be transported is via the symmetric mobile affinity forms of the transporter. Figure 1d shows that lumping the dual processes of ligand transit between phases and isomerization from high to low affinity into the single rate constants k_{15} and k_{51} obscures the necessity of equilibration of the mobile C_H (high-affinity) carrier form across the phase boundary between the external and internal membrane phases. The presence of this mobile high-affinity carrier form in both membrane phases short-circuits the isomerization reaction from the transport reaction, thereby preventing the ligand bound to the immobile low-affinity isomer from taking part in the transport process (Fig. 1d).

The Wegscheider Condition, Detailed Balance and Cyclic Equilibrium Processes

Wegscheider (Lewis 1925; Wegscheider 1901) showed that all of the reversible subreactions within a cyclic chemical process must themselves be at equilibrium at all stages of the cycle before overall equilibrium is attained. Lewis, using the example of the triple point of water, similarly demonstrated that "cyclic equilibria" do not exist. At the triple point, when the temperature is 273.16 K° water and partial water vapor pressure is 0.611 kPa, water vapor and ice are in equilibrium. Removal of ice from the mixture does not affect the equilibrium between water and water vapor.

The difference between the triple point equilibrium of water and the asymmetric carrier cyclic equilibrium is that although mass balance is maintained in all branches of the carrier cycle, energy balance is ignored. The energy shortfall between nodes 1 and 2 and between 3 and 4 in Fig. 1a has to be compensated by the energy difference between 1 and 4. In contrast, no energy difference exists between any node in the case of the triple point equilibrium with equilibrium between water, water vapor and ice and water vapor pressure. Removing the free carrier connection between nodes 1 and 4 (Fig. 1a) unbalances the equilibrium between the high- and low-affinity sites of the glucose carrier at nodes 2 and 3 as the energy difference between the bound ligands must be offset by the energy difference between vacant carrier states at nodes 1 and 4 to maintain overall mass balance.

The energies for the external$_2$ and internal$_3$ ligand carrier complex GC are obtained by application of van't Hoff's equation (Kondepudi and Prigogine 1998) to the flux ratios of the four-node model cycle (Fig. 1a).

Although assignment of asymmetric rates of carrier equilibration is an apparently convenient way of reconciling carrier asymmetry with the detailed balance constraints, it also implies that energy generated within the vacant carrier distribution offsets the energy difference due to the ligand affinity differences.

It is evident that the triple constraints of mobile carrier path cyclicity combined with asymmetric ligand affinities and the absolute requirement to maintain equimolar equilibrium in the external solutions are irreconcilable. The asymmetric rates of vacant carrier movement do not resolve the dilemma of how to compensate for the energy difference between the ligand affinities within the cyclic carrier constraints. This requires unequal vacant carrier distribution at equilibrium, i.e., failure to observe the ergodic hypothesis, which requires that particles of equal energy should have the same average density throughout any phase space to which they have access (Tolman 1925). In macroscopic terms this translates to Gibbs' phase rule

requirement that the chemical potential differences between all mobile components in all phases are zero at equilibrium.

Other Asymmetric Uniporters

The above discussion offers proof that any cyclic transport model requiring asymmetric rates of vacant-carrier movement to compensate for an energy imbalance generated by its asymmetric affinities is, without exception, invalid. Asymmetric carriers have been invoked to describe a wide variety of organic solute transport systems via uniporters, e.g., choline, (Deves and Krupka 1981; Edwards 1973), purines and nucleosides (Jarvis et al. 1983) and organic acids (Eraly 2008). All of these model systems are equally invalid for the reasons stated above.

Fixed Asymmetric Site Model of Transporters

The problems implicit in the alternating asymmetric carrier model of glucose transport are averted if the determinate mobile site assumption is relinquished and instead the transporter is assumed to consist of an array of fixed sites with asymmetric affinities which may partially occlude an interconnecting channel. Ligand flows then occur stochastically by serial jumps resulting from ligand dissociations and associations between the external solutions and vacant sites, between the ligands within the intervening occluded zone and between the ligand binding sites and any vacant binding site exposed to the central zone (Fig. 2a).

Ligand dissociation rates from low-affinity sites are proportionally faster than those from higher-affinity sites at any given ligand concentration; e.g., although glucose dissociation from a low-affinity site has a faster rate, it also has a proportionally lower fractional saturation, ϕ^{iG}. Thus, at equilibrium, when the ligand activities are equalized in the external solutions and in the intermediate occluded zone, the rates of ligand transit between any two sites will always be the same.

If at equilibrium with solution glucose concentration $G^{out} = G^{in}$ the ligand association rates with the high- and low-affinity sites are equal, then the ratio of dissociation rates from the inside site 3 and the outside site 2 are proportional to the dissociation constants

$$k_{32}/k_{21} = K_D^{in}/K_D^{out}$$

At equilibrium the unidirectional ligand fluxes between sites

$$2 \rightarrow 3 = \phi^{2G} \cdot k_{23} \cdot k_x \cdot \left(1 - \phi^{3G}\right).$$

and sites

$$3 \rightarrow 2 = \phi^{3G} \cdot k_{32} \cdot k_x \cdot \left(1 - \phi^{2G}\right). \quad (25)$$

where k_x is a rate proportional to the symmetric diffusion coefficient within channel, are equal. Therefore at equilibrium, the multisite transporter is in detailed balance (Fig. 2e, panel b).

An important physical implication of this model system is that the ligand dissociating from the high-affinity external site into the internal occluded space between sites reverts at equilibrium to the same energy level, i.e., concentration, as is present in the external solution prior to binding to the low-affinity site, or vice versa. Thus, no energy is transferred between the high- and low-affinity sites by ligand transit between sites via the intermediate space at equilibrium, and this avoids the problem of compensating for energy changes resulting from direct ligand transference between different affinity sites, as occurs with asymmetric alternating carriers. This formulation of the fixed-site model, as well as providing a good simulation of the apparent multicompartment kinetics of glucose transport (Carruthers et al. 2009; Leitch and Carruthers 2009), provides a straightforward solution to the thermodynamic problem of asymmetric affinities without violating the energy conservations laws.

Exchange Transport via Mobile or Fixed-Site Asymmetric Transporters

An attractive aspect of the alternating carrier model for glucose transport is that it rationalizes most of the phenomena related to accelerated exchange and counterflow of glucose or other ligands. *Exchange flux* here means exchange of labeled sugar ligand, initially present in the external solution with unlabeled sugar, initially present only in the cytosol, or vice versa. Exchange flux is said to be accelerated because the maximal "unidirectional" rate is faster than the maximal rate of net flux (LeFevre and LeFevre 1952). *Counterflow* is the uphill flow of labeled ligand driven by downhill flow of unlabeled ligand.

The mobile carrier explanation for accelerated ligand exchange is that the path for ligand exchange via the mobile carrier nodes ($1 \rightarrow 2 \rightarrow 3 \rightarrow 4$) and ($4 \rightarrow 3 \rightarrow 2 \rightarrow 1$) short-circuits the slow path of vacant-carrier transit ($4 \rightarrow 1$) or ($1 \rightarrow 4$) (Fig. 1a).

The glucose-exchange process, as well as having a higher rate, has a higher $K_{m(exchange)}$ than $K_{m(net\ influx)}$. This arises because both outside and inside sites must be fully saturated with labeled and unlabeled ligand, respectively, before exchange flux is maximal. Consequently, the $K_{m(equilibrium\ exchange)}$ for both carrier and fixed-site mechanisms is mainly determined by the low-affinity inside site, whereas the $K_{m(net\ influx)}$ is determined only by the high-

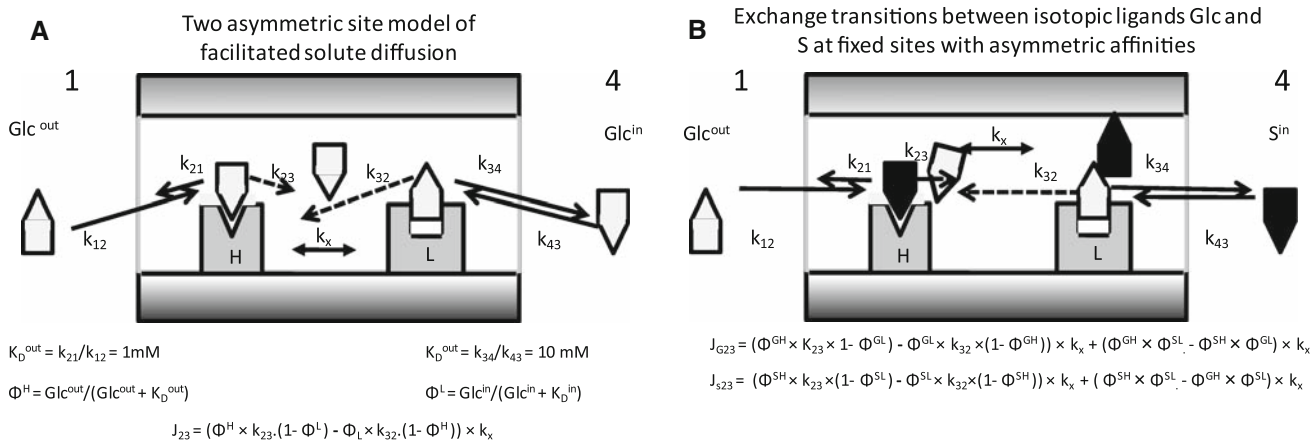

affinity external facing site (Baker and Widdas 1973) (Fig. 2b).

The fixed-site transporter model requires that accelerated exchanges between free ligand in solution or in the intersite space within the membrane and ligands bound to the transporter ligand binding sites are faster than net flux. More rapid exchange will occur between bound and free ligand, providing the "activation energy" for exchange is lower than that for the net dissociation (Fig. 2b). The lower activation energy for glucose exchange than net flux is well recognized but has been variously interpreted (Whitesell et al. 1989; Brahm 1983). If the activation energy for exchange is higher than that for net uptake and dissociation, then exchange retardation will occur, as has been

◀ **Fig. 2** **a** An illustration of the two asymmetric site model for facilitated diffusion of glucose, which closely simulates the net fluxes of glucose shown in **d** and Table 1. The high-affinity site on the outside has a $K_D = 1$ mM and the low-affinity site (L) has a $K_D = 10$ mM. The assigned rate constants for association and dissociation are the same as in Fig. 1 for the symmetric or asymmetric three-state mobile carriers. The external solution is assigned as phase 1 and the internal bathing solution, phase 4. **b** An illustration of the mode of ligand exchange between isotopes of glucose in the free solution; unlabeled glucose is present in the external solution and labeled glucose (*black*), in the inside solution. The ligands can exchange between connected sites or between the external solutions and adjacent binding sites as shown. The equations are simulated exchange fluxes shown in **d**. **c** Simulated zero-*trans* net influx and efflux via the three-node mobile carrier as illustrated in Fig. 1c with either symmetric or asymmetric affinities. Lines with positive flux values are influx rates and those with negative values are efflux rates at varying concentrations of glucose in either the external solution for influx or the internal solution for efflux. The symmetric transporter generates operational K_m values for import or export of 0.9 mM and V_m values of 0.09 s^{-1} with assigned affinities of 1 mM on each side with the rates of association and dissociation between solutions and sites 1 and 3 = 1.0 s^{-1} and the inverse rates of free-carrier transit = 0.1 s^{-1}. The asymmetric carrier is assigned a dissociation rate $k_{23} = 10$ s^{-1} and $k_{31} = 0.01$ s^{-1}; all other constants are the same as for the symmetric carrier. The operational K_m for exit is 7 mM and the V_m for net exit = 0.48 s^{-1}, whereas the K_m and V_m for net entry become 0.8 mM and 0.08 s^{-1}, respectively. These Michaelis–Menten parameters were obtained from the simulations, using Levenberg–Marquardt least square fitting in Kaleidagraph (Synergy Software, Reading, PA, http://www.synergy.com). **d** Simulation of asymmetric glucose (3-OMG) transport in erythrocytes at 4°C. The data simulated are those published by Cloherty et al. (1996) as shown in **c** and **d**. The rates and affinities were adjusted to obtain a good fit to the observed data. There are several other possible fits obtainable; however, the key points are that fitting requires asymmetric affinities with a low-affinity internal site $K_D = 12$ mM and a high-affinity external site $K_D = 0.5$ mM. It should be noted that the observed ratio of $K_m^{out}/K_m^{in} = 0.38/4.35 = 0.87 <$ the assigned ratio = 0.5/12 = 0.41. The masking of the asymmetry ratio is due to crossover of ligands between the internal and external binding sites. Infinite-*trans* exchange flux is obtained by maintaining internal unlabeled [3OMG] = 100 mM and varying external labeled [3-OMG] from 0 to 100 mM; equilibrium exchange is obtained by varying internal and external [3-OMG] from 0 to 100 mM simultaneously; zero-*trans* net entry and exit are obtained by varying the external or internal [3-OMG] from 0 to 100 mM, while maintaining the concentration in the *trans* solution at zero. Zero net flux with equimolar concentrations is obtained when external [3-OMG] and internal [3-OMG] are both varied equally and simultaneously from 0 to 100 mM. **e** Comparison of energy profiles at equilibrium of the ΔG for glucose as it traverses the transporter from outside to inside. (*a*) The change in glucose free energy as it traverses from the external solution to the high-affinity site $C^{(1)}$, where it forms a complex with carrier $GC^{(2)}$ (–17.2 kJ). It transits to the inside, gaining ΔG to form the inside low-affinity $GC^{(3)}$ complex (–11.49 kJ) before dissociation into the inside solution. During return transit, the free-carrier C^4 loses unsourced energy (5.74 kJ), which compensates for the energy gain on GC transit. (*b*) As glucose traverses the two-site transporter from outside, it first binds to a high-affinity site (–17.2 kJ), then dissociates to the intersite space, where it reverts to the same energy level as in the external solutions (0 kJ). Then, it binds to the low-affinity site (–11.49 kJ) prior to dissociation to the inside pool. No transferences of energy between the ligand binding sites occur with this model

observed with exchanges between different hexoses (Cloherty et al. 1996). The two-site model indicates that glucose exchange and net flux have different mechanisms, so this readily accounts for their different activation energies.

For the past 50 years counterflow and accelerated exchange have been used as the critically decisive criteria in support of the mobile carrier theory (Wilbrandt and Rosenberg 1961). However, this assumption of a counterflow mechanism being exclusively due to carrier kinetics requires that no other mechanism exists for more rapid ligand exchange. Faster isotope exchanges than net dissociative flux are well-recognized phenomena in chemical and biochemical catalysis. An example where rapid exchanges occur at fixed binding sites is of deuterium–hydrogen exchange on nickel catalysts: Hydrogen production and deuterium proton-exchange reactions are catalyzed by nickel (Saint-Martin et al. 1988). Hence, counterflow cannot be considered to be exclusively a characteristic of mobile carriers.

Equations for Exchange Flux

The following general equations apply to exchange between free glucose (Glc) and free labeled glucose (S) present in the external, intermediate or internal solutions and between bound glucose (GC) or bound labeled glucose (SC) present at either the external high- or internal low-affinity sites:

$$\begin{aligned}&\text{The exchange rate of } Glc^{out} \text{ with bound}\\ &SC^{out} = k_{ex} \cdot (Glc^{out} \cdot SC^{out} - S^{out} \cdot GC^{out})\\ &\text{and the exchange rate of } S^{out} \text{ with bound}\\ &GC^{out} = k_{ex} \cdot (S^{out} \cdot GC^{out} - G^{out} \cdot SC^{out})\end{aligned} \quad (26)$$

where k_{ex} is the bimolecular rate of exchange between bound and free ligands.

Hence, the total flux of Glc = J^1_{Glc} between the external solution and the external binding site is the sum of net and exchange fluxes

$$\begin{aligned}J^1_{Glc} = {} & Glc^{out} \cdot k_{01} \cdot (1 - GC^{out} - SC^{out}) - GC^{out} \cdot k_{10}\\ & + k_{ex} \cdot (Glc^{out} \cdot SC^{out} - S^{out} \cdot GC^{out})\end{aligned} \quad (27)$$

Similarly, the total flux of S = J^2_S between the external solution and the external binding site is the sum of net and exchange fluxes

$$\begin{aligned}J^2_S = {} & S^{out} \cdot k_{01} \cdot (1 - SC^{out} - GC^{out}) - SC^{out} \cdot k_{10}\\ & + k_{ex} \cdot (S^{out} \cdot GC^{out} - Glc^{out} \cdot SC^{out})\end{aligned}$$

where k_{01} is the association rate and k_{10}, the dissociation rate of ligand to and from the site, respectively.

The equations for exchange flux between the external site and intermediate solutions, the intermediate solution and the internal site and the internal site and the internal solution follow the same pattern (Carruthers et al. 2009; Naftalin 2008a).

The major differences between the equations for net and exchange kinetics via fixed multisite transporters and the alternating carrier model are that the alternating carrier model requires that "exchange" flux occurs by sequential exchanges between the ligand isotopes at either the external or the internal face of the alternating site whose affinity alters during its translocation. Thus, accelerated exchange is conventionally envisaged as a rapid isotopic shuttle process that short-circuits the slower pathway taken by the vacant carrier.

With the multisite model, exchanges between isotopic ligands are envisaged to occur between ligand bound to either of the two sites (Fig. 2a, b) and isotope present in either of the adjacent solutions on each side of the sites. Thus, exchange occurs between the external solution and its adjacent site or between the intermediate solution and either of the adjacent sites. Because of the extra degrees of freedom within the multisite model, geminate exchanges occur between the bound ligands and free ligands in the intermediate compartment. Thus, both net and exchange fluxes between the sites are modulated by the ligand concentrations in the intermediate solution and the fractional occupancy of the alternate site. This cannot occur with the single alternating carrier.

Implementation of the multisite assumptions permits all the observed kinetics of both net and exchange fluxes of glucose, including counterflow, in human erythrocytes via GLUT1, as illustrated in Fig. 2c, d and Table 1 (Leitch and Carruthers 2009; Naftalin 2008a).

The Multisite Model Elucidates the Biphasic Kinetics of Glucose Exchange

It has been known for nearly a century that although glucose enters human erythrocytes initially very rapidly, during the later stages of equilibration, at high glucose concentrations, equilibration with the cytosol is very slow, thereby rendering the cells resistant to osmotic lysis in hypotonic salt solutions (Ege 1927). Until recently, the biphasic kinetics of glucose exchange equilibration in human erythrocytes were rationalized either by the hypothesis that the faster rate of β-D-glucose uptake via the GLUT1 transporter was followed by slow rates of anomerization of β- to α-D-glucose anomer in the cytosol or by multicompartmental glucose distribution within the cytosol. Neither explanation is satisfactory. Increasing glucose anomerization rates by 100-fold by extracellular anomerizing enzyme had no effect on the biphasic glucose uptake kinetics, and furthermore, no evidence exists for intracellular compartmentalization of other solutes.

Simulating glucose-exchange kinetics with the multisite model outlined in Eqs. 26 and 27 and Fig. 2a, b produces an excellent fit to the observed biphasic kinetics in control conditions and with unilateral inhibitors applied (Fig. 2d) (Leitch and Carruthers 2009). The explanation for the biphasic kinetics of labeled glucose uptake into cells preloaded with unlabeled glucose is that exchange uptake is initially very fast because the inside site is saturated with unlabeled glucose. However, as the cytosol begins to accumulate labeled glucose, it binds to both external and internal sites and accumulates within the intermediate space, so geminate exchanges of labeled glucose occur with increasing frequency (Carruthers et al. 2009; Leitch and Carruthers 2009). This "geminate exchange" process slows the apparent exchange rate and accounts for the second slow phase of exchange. When the external site is occupied with inhibitor, e.g., phloretin, the initial rate of exchange uptake is reduced and reduces geminate exchange, thereby preventing the apparent biphasic exchange kinetics.

These experiments are useful corroborations of the multisite kinetic scheme since the alternating carrier model does not simulate the two-phase exchange uptake process without assuming a multicompartmental cytosol or membrane.

Conventional Cotransport Models

The Primary Thermodynamic Inconsistency of Conventional Cotransport Models

A fundamental assumption of symport and antiport cotransport mechanisms based on the conventional determinate single alternating-site paradigm is that the static head equilibrium condition is maintained by a balance of equal and opposite forces generated by inverse concentration ratios of the driving and driven ligands across the common pathway for the cotransported ligands complexed with the carrier (Fig. 3a, b, e, f). Static head is assumed to result from complexation of both cotransported ligands with the alternating carrier at least for the duration of the alternating switch process. The combined potential gradient of these transiently bound ligands is assumed to generate the force for cotransport. The two or more transported ligands are assumed to be linked together stoichiometrically, similarly to the way in which the electrical and chemical potentials of a fixed ion, like Na^+, are conjoined to generate the combined electrical and chemical potential components of the electrochemical potential. The symport device is assumed to act as an energy lever that both aggregates the combined potentials of the cotransported

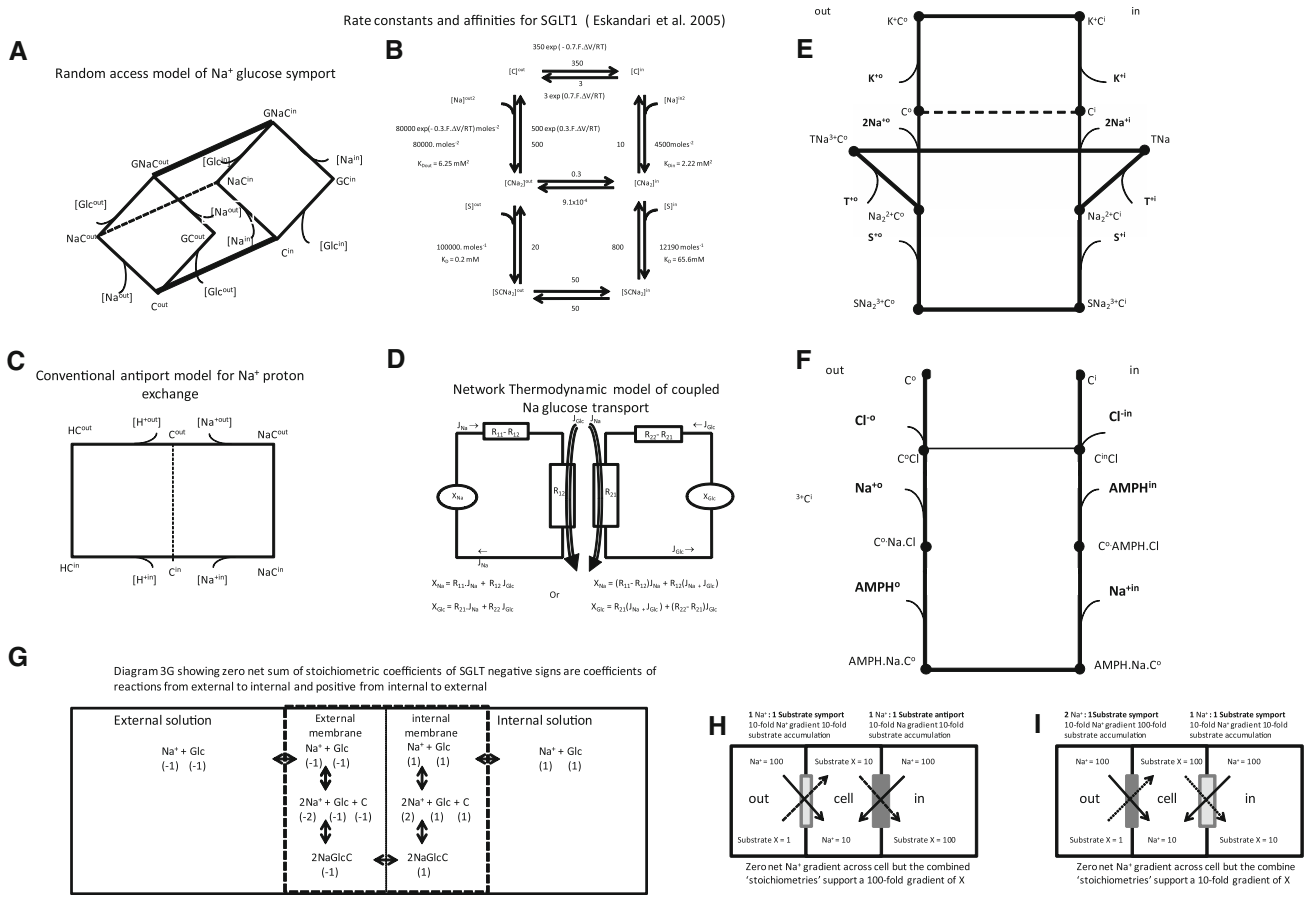

Fig. 3 **a** The model shows the pathways of random access Na^+ and glucose binding to Na^+–glucose cotransporter as outlined by Turner (1981). The primary and secondary dissociation constants of Na^+ and glucose binding to the sites on the inside and outside are shown. *Dotted line* illustrates one possible leak route for Na^+. The presence of this pathway alters the equilibrium constraints of the carrier. **b** The rate constants and affinities of ordered α-methyl-glucoside (αMG) and Na^+ addition at the inside and outside faces of the sodium–glucose cotransporter SGLT1 (Eskandari et al. 2005). At the external surface the observed $K_{0.5}^{\alpha MG} = 0.33$ mM at 100 mM Na^+ and $K_{0.5}^{Na} = 54$ mM at 1 mM αMG. **c** Conventional antiporter model for Na^+ and proton exchange. *Dotted line* shows the leak pathway for vacant carrier. **d** Network thermodynamic model of a linear Na^+–glucose cotransporter (adapted from Mikulecky, 2001). The network shows a resistance, rather than a conductance, formulation, as is more usual (where $R_i = 1/L_i$), as in the text. It can be seen that the Na and glucose circuits are separate but interact via the transducer element, which couples the flows of Na^+ and glucose. The net driving forces on Na^+ and glucose are only those available from the electrochemical potential gradients between the external pools X_{Na} and X_G. **e** Conventional alternating single-site model of serotonin cotransport, SERT, with a symporter of $2Na^+$:1 serotonin coupled with an antiporter for K^+ as proposed by Rudnick (2006). The out-of-plane pathway provides a route for Na_2:serotonin:Na_2 serotonin label exchange. *Dotted line* shows the slow rate of vacant carrier movement across the membrane plane and provides the facility for an uncoupled K^+ leak. **f** Diagram showing an alternative alternating carrier cotransport model in which Na^+, Cl^- and amphetamine (AMPH) are coupled as proposed by Erreger et al. (2008). It is assumed that the vacant carrier is unable to cross the membrane. **g–i** Two results of "thought experiments" where a cell layer is the interface between two external solutions. In **e** the external cell membrane has a 1:1 Na^+ substrate *x* symporter and the internal cell membrane has a 1:1 Na^+ substrate *x* antiporter. The internal and external solutions have NaCl concentration = 100 mM, the cytosol has NaCl concentration = 10 mM and the substrate *x* has a concentration = 1, 10 and 100 mM in the external cell and internal solutions, respectively. In **f** the external symporter has a stoichiometry of $2Na^+$:1X, whereas the transporter in the inner membrane now is a symporter with a stoichiometry of $1Na^+$:1X. The external NaCl concentrations are 100 mM and the cell NaCl, 10 mM, as in **e**. However, the substrate X concentrations are 1,100 and 10 mM. Although there is no Na^+ driving force between the external and internal solution compartments, the "static head" equilibria permit a stationary uphill accumulation of substrate X between the inside and outside pools. It is seen that apparently only the difference in stoichiometric coefficients of the cotransporters is required to maintain a static head gradient across the membrane ensemble. Thus, it would appear that the stoichiometric coefficient is a source of energy. The solution to these paradoxical and clearly impossible situations is that the stoichiometric coefficients are assumed to apply only in one direction. However, stoichiometric coefficients are vectorial, so a transmembrane flow must have both inflow and outflow components which are positive and negative as they enter and leave the membrane from both sides. The conservation laws require that these stoichiometric coefficients must sum to zero for all independent flows between dissociated ligands in the external solutions. Hence, as the overall stoichiometry of the flow reactions is zero, static head equilibrium has no reality (Prigogine 1968)

ligands and funnels them into a single path through which they pass in undeviating combination.

Thus, for Na–glucose cotransport via SGLT1 (Fig. 3a, b) the free energy difference of the ligand carrier complex is

$$\Delta G_{GNaC} = \Delta G_{Glc} + \Delta G_{Na} + \Delta G_{carrier} \quad (28)$$

The entropy production rate (d_iS/dt) of any transport process is determined by the sum of the products of the ligand fluxes (J_i, mole cm^{-2} s^{-1}) and the conjugate forces (X_i, joules/mole) which generate the energy flow ($J_i \cdot X_i$, joules cm^{-2} s^{-1}).

Thus, for Na^+–glucose symport,

$$d_iS/dt = nJ_{Na} \cdot X_{Na} + J_{Glc} \cdot X_{Glc} \quad (29)$$

where $X_{Na} = nRTLn\frac{[Na]^{out}}{[Na]^{in}}$ and $X_{Glc} = RTLn\frac{[Glc]^{out}}{[Glc]^{in}}$ are the chemical potential energy gradients and n is the stoichiometric coefficient of Na^+ interaction with the cotransporter, generally assumed to be 2 for SGLT1 (Chen et al. 1995).

At static head, when both $nJ_{Na} = J_G = 0$, it follows from Eq. 29 that $d_iS/dt = 0$. Thus, the conventional cotransport model is based on the premise that the canonical cotransport mechanism is a perfectly energy-efficient process with rigid stoichiometric relationships between driving and driven ligand flows (Fig. 3a, b).

This view considers the membrane transport system in isolation from the external solutions and discounts the fact that the cotransported ions and organic substrates behave as dissociated solute species in the external solutions and only the chemical potential gradients exerted by the solutes between the external solutions exert driving forces on either coupled or uncoupled flows across the membrane (Fig. 3g) (see below).

The conventional cotransport theory with both symport and antiport assumes that any leakages of ligands, independent of their cotransported partner(s) observed experimentally, must occur outside the canonical cotransport path and are treated as separate short-circuiting leak routes, which reduce the efficiency of the otherwise perfectly efficient cotransport process (Chen et al. 1997; Eddy 1982; Eskandari et al. 2005; Mackenzie et al. 1998; Panayotova-Heiermann et al. 1995; Semenza et al. 1985) (Fig. 3a, b).

Thus, in the sodium–glucose cotransporter model, an Na_2 leak, namely, $2Na^+$ bound to carrier without glucose, short-circuits the Na_2–glucose carrier complex primarily by reducing the potential for the cotransporter to accumulate glucose against a concentration gradient. A 1% Na_2 leak rate reduces the maximal accumulation ratio from 100-fold to fourfold and a 10% Na_2 leakage reduces the maximal glucose accumulation to 1.34% of that predicted in the case of a leak-free transporter. The model of cotransport illustrated in Fig. 3b actually assumes an asymmetric Na_2 leak, so it does not have this disadvantage as the asymmetry of the leak fluxes prevents buildup of the complex Na_2GC^{in} which would otherwise occur with the symmetric Na_2C leakage (Fig. 4g). On the other hand, this asymmetry assumption requires the additional assumption that the rates of passively mediated Na_2C can be asymmetric (see below and the previous discussion on asymmetry).

Symport

Cotransport systems are necessarily more complex than uniporter facilitated diffusion systems as they involve more ligands, which may form and dissociate in an ordered or random sequence. Additionally, polyvalent stoichiometries and electrical potential have been invoked to explain cotransport kinetics. Electrical potential is presumed to alter not only the mobilities of charged ligands but also the transit rates of vacant and liganded carriers and the unilateral rates of formation of ligand carrier complexes (Eskandari et al. 2005; Zomot et al. 2007). These factors greatly increase the complexity of the symporter kinetic equations, which makes intuitive understanding difficult. Turner (1981) examined the kinetics of random addition of two ligands to a symporter with 1:1 stoichiometry but not the full thermodynamic implications of this cotransport model (Fig. 3a). Although the kinetics of cotransport are complex, the thermodynamics of formation of the canonical cotransport complex are relatively simple and their implications will be explored.

Detailed Balance with Randomly Ordered Binding of Two Ligands to the Mobile Complex

Coupled flow between two ligands via an alternating cyclic carrier is portrayed as arising because the ligand transport cycles have a common branch shared between the carrier and the two cotransported ligands. Thus, a transmembrane gradient of a ligand, e.g., Na^+, will also generate a stoichiometric transmembrane flow of glucose and an intramembranous flow of carrier via this assigned cotransport path, even if either no gradient or a negative gradient of these components is present (Fig. 3a, b). As a corollary, when the gradient of the tertiary ligand carrier complex in SGLT is nullified by equal concentrations or "electrochemical potentials" of GNaC at the inner and outer faces of the transporter, there is zero net flow of both ligands via this pathway. This is called the "static head equilibrium condition."

Randomly ordered ligand association with the carrier implies that binding of either Na^+ or glucose first requires the alternate ligand to bind next to form the mobile ternary complex. Stepwise additions of the alternate ligand pairs to the carrier at each side generate converging paths to the

tertiary complex $GNaC^{i}$. Detailed balance requires that the products of the ligand affinities via both pathways leading to formation of the same complex are equal (Fig. 3a) (Eqs. 28–37).

Detailed Balance and the Law of Mass Action

Detailed balance and the law of mass action require

$$[Na]^{out} \cdot C^{out} \cdot k^{f}_{Na} = NaC^{out} \cdot k^{r}_{Na} \text{ or } [Na]^{out} \cdot C^{out} = NaC^{out} \cdot K^{out}_{D_{Na}} \quad (30)$$

where the dissociation constant of Na^+ for the external carrier site is $K^{out}_{D_{Na}} = k^{r}_{Na}/k^{f}_{Na}$. Similarly, the glucose dissociation constant for the external carrier site is $K_{D^{out}_{G}} = k^{r}_{G}/k^{f}_{G}$, and

$$[Glc]^{out} \cdot C^{out} \cdot k^{f}_{G} = GC^{out} \cdot k^{r}_{G} \text{ or } [Glc]^{out} \cdot C^{out} = GC^{out} \cdot K_{D^{out}_{G}} \quad (31)$$

Detailed balance requires

$$[Na]^{out} \cdot GC^{out} = GNaC^{out} \cdot K_{D^{out}_{Na}} \text{ and } [Glc]^{out} \cdot NaC^{out} = GNaC^{out} \cdot K_{D^{out}_{G}} \quad (32)$$

$$\text{Thus, } GNaC^{out} = \frac{[Na]^{out} \cdot GC^{out}}{K^{out}_{D_{Na}}} = \frac{NaC^{out}}{K^{out}_{D_{G}}} \quad (33)$$

Equations 31–33 give

$$GNaC^{out} = \frac{[Na]^{out} \cdot [G]^{out} \cdot C^{out}}{K^{out}_{D_{Na1}} \cdot K^{out}_{D_{G2}}} = \frac{[Na]^{out} \cdot [G]^{out} \cdot C^{out}}{K^{out}_{D_{G1}} \cdot K^{out}_{D_{Na2}}} \quad (34)$$

$$\text{Hence } K^{out}_{D_{Na1}} \cdot K^{out}_{D_{G2}} = K^{out}_{D_{G1}} \cdot K^{out}_{D_{Na2}} \quad (35)$$

The same relations as in Eqs. 33–35 hold for the inside sites:

$$K^{in}_{D_{Na1}} \cdot K^{in}_{D_{G1}} = K^{in}_{D_{G1}} \cdot K^{out}_{D_{Na2}} \quad (36)$$

At static head equilibrium, with a symmetric alternating symporter, the same relations hold as for the symmetric uniport transporter; hence, from Eqs. 6–9

$$C^{in} = C^{out} \text{ and } GNaC^{out} = GNaC^{in} \quad (37)$$

$$K^{out}_{D_{Na1}} \cdot K^{out}_{D_{G2}} = K^{out}_{D_{G1}} \cdot K^{out}_{D_{Na2}} = K^{in}_{D_{Na1}} \cdot K^{in}_{D_{G2}} = K^{in}_{D_{G1}} \cdot K^{in}_{D_{Na2}} \quad (38)$$

$$[Na]^{out} \cdot [G]^{out} \cdot C^{out} = [Na]^{in}, [G]^{in}, C^{out} \text{ or } \frac{[Na]^{out}}{[Na]^{in}} = \frac{[G]^{in}}{[G]^{out}} \quad (39)$$

Equation 39 demonstrates the static head equilibrium condition.

Problems with Leak Pathways

As the determinate model of cotransport enforces rigid stoichiometric coupling of the cotransported ligand flows via a single pathway, it follows that any uncoupled flows are considered as leaks via alternative routes. The tightness of cotransport coupling can be viewed as an aspect of the capacity or "selectivity" (Krupka 1990) of the carrier to prevent either of the single ligands, glucose or Na^+, from equilibrating across the transporter via "leak" pathways. Incorporating leakage within the cotransport models of either ligand implies additional constraints and therefore new detailed balance conditions. If a leak pathway exists because Na^+ equilibrates via the complex NaC^{i} along the branch (dotted line Fig. 3a), this generates two additional cycles with additional constraints to overall detailed balance. These two cycles are

$$C^{out} \leftrightarrow NaC^{out} \leftrightarrow NaC^{in} \leftrightarrow C^{in} \leftrightarrow C^{out} \text{ and } NaC^{out} \leftrightarrow GNaC^{out} \leftrightarrow GNaC^{in} \leftrightarrow NaC^{in} \leftrightarrow NaC^{out} \quad (40)$$

Since NaC can now equilibrate between the inside and outside of the membrane, equilibrium between inside and outside phases requires that the activities (a) of the equilibrating states should be equal:

$$aC^{in} = aC^{out} \text{ and } aGNaC^{out} = aGNaC^{in} \text{ and also } aNaC^{out} = aNaC^{in} \quad (41)$$

This third constraint reduces the number of degrees of freedom of the static head condition. Now, detailed balance requires that both $[Na]^{out} = [Na]^{in}$ and $K^{out}_{D_{Na1}} \cdot K^{in}_{D_{Na1}}$.

Thus, when leaks of either ligand are factored into the cotransport model, the only equilibrium that can exist is when the solutions on both sides of the transporter have equal ligand concentrations. Put more simply, any leakage is incompatible with static head equilibrium.

Additional Problems Relating to the Eskandari Model of Asymmetric Cotransport

The Asymmetry Problem

The Eskandari model of cotransport of glucose and Na^+ is asymmetric, with a 117-fold lower internal affinity for ligands than at the external site (Eskandari et al. 2005). The asymmetry rationalizes the very much slower observed glucose export flux against the direction of the Na^+ electrochemical potential gradient than predicted on the basis of the energy generated by the Na^+ electrochemical potential difference between the bathing solutions and the relative insensitivity of the model to substantial Na leakage rates (Holman and Naftalin 1976). As shown in Fig. 3b, the model is an ordered bi–bi reaction, where 2 mol of Na^+

bind prior to 1 mol of glucose, followed by symmetric translocation of the Na_2GC complex and ordered release of 2 mol of Na^+, followed by 1 mol of glucose.

The dissociation constants at the external and internal sites for Na_2 and glucose are

$$K^{out}_{D_{Na1}} = 500/80,000 = 6.25\,mM^2 \text{ and } K^{in}_{D_{Na1}} = 10/4,500 = 2.22\,mM^2$$

$$K^{out}_{D_{G2}} = 20/10,000 = 0.2\,mM \text{ and } K^{in}_{D_{G2}} = 800/12,190 = 65.62\,mM$$

$$\text{Thus } K^{out}_{D_{Na1}} \cdot K^{out}_{D_{G2}} = 6.25 \times 0.2 = 1.25\,mM^3$$

$$\text{and } K^{in}_{D_{Na1}} \cdot K^{in}_{D_{G2}} = 2.22 \times 65.62 = 145.67\,mM^3$$

The asymmetric affinities are balanced by matching asymmetries for both the vacant carrier transits of $\frac{\text{inflow rate}}{\text{outflow rate}} = \frac{350}{3} = 11.87\,kJ$ and are also sustained by asymmetric rates of the carrier–Na_2 complex at zero PD $\frac{\text{inflow rate}}{\text{outflow rate}} = \frac{0.3}{9.1\times10^{-4}} \cong 14.5\,kJ$.

An implicit assumption of this model, as with the asymmetric alternating carrier theory for uniport glucose transport, is that energy sources are needed to sustain the asymmetric affinities of the cotransporter system for Na_2 and glucose and for the divalent Na_2–carrier complex.

The major advantage of the asymmetric rates of Na^2C carrier leakage is that the asymmetric Na leak prevents the very substantial reductions in the static head equilibrium seen with symmetric leaks as shown in Fig. 4f, g (Eskandari et al. 2005; Mackenzie et al. 1996, 1998; Panayotova-Heiermann et al. 1995). However, while this asymmetry is consistent with "detailed balance," it requires an exogenous and imaginary energy source to sustain it.

The Stoichiometry Problem

The Eskandari model of Na–glucose cotransport via SGLT1 (Eskandari et al. 2005) assumes that 2 mol of Na^+ for every mole of glucose bind to each face of the mobile carrier. The energy gradients are $X_{Na} = nRTLn\frac{[Na]^{out}}{[Na]^{in}}$ and $X_G = RTLn\frac{[G]^{out}}{[G]^{in}}$, where n is the stoichiometric coefficient of Na^+ binding to the mobile complex, generally assumed to be 1 or 2.

If it is assumed that there are no leaks, then within the membrane microenvironment the energy gradient across the transporter for $Na^+ = nRTLn\frac{[Na]^{out}}{[Na]^{in}}$. However, the real thermodynamic driving forces for transport exist only between source and sink pools in the external and internal solutions. In these external solutions Na^+ and glucose exist only in a dissociated state, free of any binding associations with other ligands or membrane components. Even when Na^+ transit across the transporter is exclusively via a Na_2GC complex without leakage, the net transport process via SGLT requires that this complex formation on the *cis* side is entirely reversed when the ligands are released into the adjacent *trans* solutions. Because of assigned reversibility of the model ligand flows via the cotransport, the total stoichiometry of the ligand transporter reactions requires summation of both associative reactions on the *cis* side, which have positive signs, and dissociative reactions on the *trans* side, which have negative signs. Consequently, summing all the positive and negative valence coefficients in the stoichiometric matrix must always have a zero net valance (Prigogine 1968) (Fig. 3g). Where there is a series of reactions with neither net ligand consumption nor generation, such as occurs in any equilibrative transport process, the net valence coefficient of the overall process is always zero. This precludes the existence of any stoichiometric relationship of the ligand flows between the source and sink solutions.

Any ligand complexes formed within the membrane are only transitory intermediates between the start reactions with source ligands and end reactions yielding products with sink ligands. These initial and final reactions consist of both Na^+ and glucose entry or exit from the membrane via unconnected diffusive processes. Consequently, the only driving forces impelling the ligand flows through the reversible reactions within the membrane are the electrochemical potential gradients of these ligands, existing between the external solutions on either side of the membrane and not the converse condition, as is the explicit and erroneous assumption with most conventional determinate cotransporter models.

Antiporter Models

The conventional antiporter model, e.g., for Na^+:H^+ exchange (Fig. 3c) and K^+ dependence of serotonin accumulation (Fig. 3e) as with all other determinate alternating carrier models, proposes that a single binding site alternates between exposure to the inside and outside surfaces. The model for Na^+/proton exchange implies that a downhill thermodynamic force of Na^+ movement acts via the antiporter to drive uphill proton movement in exchange flux mode. The ideal condition for this obligatory exchange flux requires that the vacant carrier form does not transit between the alternate sides. While obligatory exchange is the standard operating mode in a wide variety of exchange transporters, slower net flux modes have been observed frequently. Net flux cycles of either or both Na^+ or H^+ are possible only if the vacant transporter is able to transit the transporter. This is usually interpreted as being due to the transporter having a second "channel mode" of operation in addition to the carrier exchange mode without net flow. Net flow can occur only if the vacant carrier crosses the transporter (Eraly 2008).

Obligatory exchange of charged species pairs, e.g., Na^+/H^+ (Olkhova et al. 2006), Cl^-/HCO_3^- (Ellory et al. 2009) and nNa^+/Ca^{2+} (DiPolo and Beauge 2006), is assumed to occur because the vacant carrier either does not cross or crosses much less frequently than the independent ligand complexes as a separate "channel" mode.

Application of the law of mass action to the conventional antiport model requires

$$[Na]^{out} \cdot C^{out} = NaC^{out} \text{ and } [H]^{out} \cdot C^{out} = HC^{out} \quad (42)$$

Similarly,

$$[Na]^{in} \cdot C^{in} = NaC^{in} \text{ and } [H]^{in} \cdot C^{in} = HC^{in} \quad (43)$$

$$\text{Thus } \frac{HC^{in}}{[H]^{in}} = \frac{NaC^{in}}{[Na]^{in}} \text{ and } \frac{HC^{out}}{[H]^{out}} = \frac{NaC^{out}}{[Na]^{out}} \quad (44)$$

$$\text{Since at equilibrium } NaC^{in} = NaC^{out} \text{ and } HC^{in} = HC^{out},$$

$$\text{at static head equilibrium } \frac{HC^{out}}{[H]^{in}} = \frac{NaC^{in}}{[Na]^{out}} \quad (45)$$

If independent net flux of either ligand is permitted, since this implies that vacant carrier (C) is now a mobile component, at equilibrium its chemical potential difference across the transporter must be zero, i.e., $C^{in} = C^{out}$. With this constraint added to Eqs. 42 and 43

$$NaC^{in} = NaC^{out} \text{ and } HC^{in} = HC^{out} \text{ only occur when}$$

$$[H^+]^{out} = [H^+]^{in} \text{ and } [Na^+]^{out} = [Na^+]^{in}. \quad (46)$$

Thus, where net flux of either ligand occurs, true equilibrium is the only condition that conforms to the constraints of the antiporter model and static head equilibrium does not exist.

All the processes described in terms of the determinate exchange transport mechanism model shown in Fig. 3c can also be described by similar exchange processes to those for stochastic model for glucose exchange shown in Fig. 2b. Thus, serial exchanges of free ligands in the solutions on either side of a binding site within an occluded channel provide an alternative explanation for antiport kinetics. This model permits asymmetric affinities without violating the energy conservation laws since no asymmetric rates of vacant carrier movement are required.

Neurotransmitter Cotransport Models Combining Symport and Antiport

Neurotransmitter transport proteins, e.g., dopamine, (DA) serotonin (5-HT), noradrenaline (NE) and gamma-aminobutyric acid (GABA), have > 50% sequence similarity (Dutzler 2007; Rudnick 2006; Sulzer et al. 2005). Their main physiological activity is neurotransmitter reuptake into neurons from the synaptic cleft after release from neuronal synaptic membranes. This reuptake activity can be subverted by drug action either to reduce uptake or to enhance neurotransmitter efflux, thereby altering their concentration and residence time in the synaptic cleft and, hence, their effect on neural signaling.

Although the membrane potentials in neurons are nearly double those observed in epithelial cells, neurotransmitter accumulations in nerve cells generally exceed sugar accumulation seen in epithelial cells by more than two to three orders and are obtained with the normal Na^+, K^+ and Cl^- concentration distributions across the cell membranes. While the physiological concentration of neurotransmitters in extracellular fluid is in the range 0.1–1 μM, the intracellular or intravesicular neurotransmitter concentration is typically in the range 1–10 mM or higher.

These very large accumulation ratios require a satisfactory explanation. The conventional models for neurotransmitter cotransport invoke multiple stoichiometries, usually two Na^+ ions, and additional force is obtained either from conjoined forces driven by a K^+ antiport or Cl^- symport (Fig. 3e, f). Thus, a 10-fold outside–inside Na^+ gradient and a 10-fold inside–outside K^+ gradient, with an overall molar stoichiometry of $2Na^+$:$1K^+$:1 5-HT, can maintain a static head gradient of 5-HT of 1,000:1 (Fig. 5c). A K^+ gradient may not be a necessity since an H^+ gradient can act as a substitute in its absence (Nelson and Rudnick 1979; Rudnick and Nelson 1978). The steady-state 5-HT gradient, although large, is exceeded by two to three orders by the neural glycine cotransporter GlyT2a (Supplisson and Roux 2002), which has a stoichiometry of $3Na^+$:$1Cl^-$:1Gly. Other neurotransmitters, e.g., GABA, also can additively couple the transmembrane Cl^- gradient to the Na^+ gradient to enhance the symport drive (Hilgemann and Lu 1999; Kanner 1978).

Concentration ratios of more than a million of glutamate between intra- and extracellular fluid are observed with 10 nM extracellular glutamate in the synaptic cleft and neural intracellular concentration of 12 mM. These are modeled by symport of 1 mol glutamate per mole H^+ and 3 mol Na^+ and one mole K^+, as estimated by monitoring the ion dependence of the reversal potential of the glutamate-dependent currents across human glial glutamate transporter GLT-1 EAAT2 in Chinese hamster ovary cells or EAAT3 in *Xenopus* oocytes (Levy et al. 1998; Zerangue and Kavanaugh 1996).

The Models for 5-HT Transport

The two alternating carrier models for Na^+ and K^+ or Na^+ and Cl^- driven neurotransmitter fluxes illustrated in Fig. 3e, f show the conventional cyclic diagrams of ligand and Na^+ binding forming a mobile carrier complex on

either side of the membrane. Carrier return is linked either to a K^+ antiport (Fig. 3) or to a Cl^- cotransport complex (Fig. 3f). Typically, neurotransmitter coupling with K^+ is observed only in the presence of Na^+ (Nelson and Rudnick 1979; Rudnick and Nelson 1978). The absence of a K^+ gradient–activated serotonin accumulation in Na^+-free conditions has been attributed to a separate pathway for K^+ via the antiport loop. This return path bypasses the vacant carrier link, which would permit uncoupled K^+ flux from the Na^+–serotonin cotransport cycle and thereby reduce the amount of energy available for cotransport, as illustrated in Fig. 5d. Similar rationalizations have been used to explain the complex role of Cl^- in amphetamine (AMPH)–DA cotransport across the DA transporter, DAT (Erreger et al. 2008). It has been suggested that Cl^- acts as both a symporter and an antiporter. In the Erreger model, Cl^- cycles around the long $NaCl^-$dependent symport route faster than across the Cl^- antiport conductance route, so an inwardly directed Cl^- gradient affects the transients generated by DA/AMPH influx but has a relatively small effect on steady-state flows and accumulation.

Simulation with the models in Fig. 3e, f indicates that the combined effect of a normal outward K^+ gradient, 110 mM internal K^+ and 5 mM external K^+, alone gives an additive force to the Na^+ gradient to generate a 1,000-fold 5-HT accumulation, whereas the Na^+ gradient with 1 for 1 stoichiometry produces only an 80-fold accumulation (Fig. 5c, e). Substantial net "leak" fluxes of either Na^+ or K^+ or 5-HT imply that the vacant carrier is able to traverse the network alone and thereby short-circuit the force-generating pathways. If free carrier movement is permitted at equal rates to the K^+-carrier movement, then the maximal 5-HT accumulation permitted by the combined K^+ and Na^+ gradients, assuming a stoichiometry of 1 Na^+ per mole 5-HT, is 100 instead of 1,000. Thus, "leakage" of free carrier reduces the efficiency of the conventional SERT carrier, just as it does with Na^+–glucose cotransport via SGLT (Fig. 4f, g).

The Necessity for New Models of Na^+–Glucose Cotransport and Na^+ Neurotransmitter Cotransport

Viable alternative schema are needed to explain both the very large steady-state neurotransmitter accumulations driven by ion gradients without resorting to asymmetric rates of vacant carrier movements or "stoichiometric" gearing and assumptions of lossless energy coupling as invoked by the conventional determinate models. Additionally, new cotransport models are required to explain phenomena that conventional models do not.

A Simple Model of Frictionally Coupled Cotransport

Conventional cotransport models require that the mobile ligand multicomplex be focused around a single site. A perceived advantage of this model is the centrally located alternating site occluding the central channel, thereby preventing ligand leakage. Coupled ligand flows arise simply by complexation of these transported ligands with different stoichiometries and affinities on the alternate sides. The main constraint on these models is of detailed balance. No real theoretical limit is set on the stoichiometric relationships between ligands, and hence, in theory an almost infinite ligand accumulation may be achieved with a sufficiently high stoichiometric relationship (n) between driving and driven ligands. These determinate models of coupling differ from the view generally taken in physical science that energy coupling between molecules is exerted by frictional interactions rather than chemical complexation (Kondepudi and Prigogine 1998; Prigogine 1968).

Onsager's (1931a, 1931b) phenomenological equations describe friction-coupled flow processes. Application of these equations to Na^+–glucose interaction gives

$$J_{Glc} = L_{Glc} \cdot X_{Glc} + L_{G-Na} \cdot X_{Na}$$
$$J_{Na} = L_{Na-G} \cdot X_{Glc} + L_{Na} \cdot X_{Na} \quad (47)$$

The fluxes J_i and forces X_i are as defined in Eqs. 29 and 47 and can be represented diagrammatically using the symbols designed for network thermodynamics (Fig. 3d) (Mikulecky 2001). The conductance matrix L_{ij} units (mole joule^{-1} s^{-1} cm^{-2}) define the frictional interactions encountered when, e.g., Na^+ and glucose interact frictionally with the membrane and the cross, or coupling, coefficients L_{ij} define the additional friction encountered when Na^+ and glucose interact within the transporter.

Onsager derived an important simplification of the phenomenological equations by showing that the cross-coefficients in the near-equilibrium condition are equal, i.e., $L_{ij} = L_{ji}$. Peusner (Mikulecky 2001; Peusner 1986) improved and extended the applicability of Onsager's relationship by showing topologically that the equality of the cross-coefficients ultimately derives from Newton's third law—"to every action there is an equal and opposite reaction"—and applies to sets of conditions far outside the near-equilibrium condition. Thus, in Eq. 47, $L_{Na-G} = L_{G-Na}$ applies over a wide glucose concentration range and far from equilibrium.

Because frictional coupling can never be completely efficient, independent ligand leakage, or "slippage," is intrinsic to frictionally coupled interactions. This contrasts with the conventional view of stoichiometrically coupled transport, where slippage is an extrinsic problem and is discounted by subtracting the uncoupled baseline flows

from the coupled flow components (Chen et al. 1995, 1997; Eskandari et al. 2005).

In the linear model of Na^+–glucose cotransport shown in Eq. 47, maintenance of a zero net glucose flow state, $J_{Glc} = 0$, with a glucose concentration difference across a membrane, $\Delta Glc \neq 0$, necessitates a continuous finite Na^+ flow, i.e., $J_{Na} \neq 0$. A finite Na^+ flow is intrinsic to the coupling mechanism and not the result of an extrinsic leak. Furthermore, because frictional interactions do not involve a fixed stoichiometric coupling, the flux ratio J_{Glc}/J_{Na} will vary with the forces of the interacting ligands generated by the electrochemical gradients existing between the source and sink pools, rather than having a fixed ratio as with stoichiometric coupling.

Expressions have been derived for the individual frictional interactions from the solute conductance coefficients for solutes and water in artificial membranes (Ginzburg and Katchalsky 1963). Unfortunately, this approach has not so far been applied to descriptions of ligand fluxes via biological transporters. However, as will be shown, the Onsager phenomenological equations can be readily used to describe biological, saturable coupled transport processes quantitatively.

The efficiency of any coupling process is measured by the fraction of entropy production of the driving process (here, the Na^+ gradient) transferred to the driven process (uphill glucose flow) (Kedem and Caplan 1965).

The main limitation of the coupling process is contained within the relationship defined as the coupling coefficient, q. This restrictive condition, which prevents efficiency from ever reaching 100%, requires that $L_{GNa} \leq \sqrt{L_{Glc}L_{Na}}$.

The overall coupling coefficient for Eq. 47 is

$$q = L_{G-Na} \Big/ \sqrt{L_{Glc} \cdot L_{Na}} \tag{48}$$

where $-1 \leq q \geq 1$. The sign of q depends on whether coupling force acts in the same direction (symport) or the opposite direction (antiport) as the driving force.

The efficiency function, η, of the cotransport process

$$\eta = -J_{Glc} \cdot X_{Glc}/J_{Na} \cdot X_{Na} \tag{49}$$

This function, η, is the fractional entropy outflow per unit entropy inflow. The maximal efficiency, η_{max}, is determined as follows (Kedem and Caplan 1965):

$$\eta_{max} = q^2 \Big/ \left(1 - \sqrt{(1-q)}\right)^2 \tag{50}$$

The network thermodynamic diagram of cotransport (Fig. 3d) shows that the kinetic energy resulting from collisions between the mobile ligands within the transporter also affects the rates and directions of flow of the other mobile components. The diagram illustrates that Na^+ and glucose flows are coupled in the transducing elements, which transform some of the energy generated by the frictional interactions of Na^+ flow into a vectorial force that drives glucose flow and vice versa. This linkage between Na^+ and glucose flows has a quasi-stoichiometric relationship between the separate flows but cannot be considered as truly stoichiometric with all that this implies in relation to mechanism.

A frictional model of coupled Na^+ and glucose flow via a Na–glucose cotransporter into a cell where the intracellular Na^+ is maintained by the action of an Na^+ pump is shown in Fig. 4i, j and illustrates the differences and similarities between the frictional models of cotransport and the conventional stoichiometric models. A similar model was described by Prigogine (1968).

Since glucose accumulates until it reaches a stationary state when $J_G = 0$, it follows from Eq. 47 that the static head condition for zero net glucose flux occurs when

$$L_{G-Na} \cdot X_{Na} = -L_G X_G \text{ or } -X_G/X_{Na} = L_{G-Na}/L_G \tag{51}$$

From Eq. 51, it follows that the maximal accumulation ratio

$$G_{in}/G_{out} = \left(\frac{[Na]^{out}}{[Na]^{in}}\right) \cdot e^{\frac{L_{G-Na}}{L_G}}$$

The maximal accumulation ratio of glucose via the transporter is proportional to the product of inwardly directed Na^+ gradient and the exponential of the ratio of the coupling coefficient L_{G-Na} to the straight coefficient of glucose permeability.

When the coupling coefficient $L_{G-Na} = 0$, Na^+ entry has no effect on glucose flux. However, when $L_{G-Na} > 0$, providing there is a positive driving force from Na^+, glucose inflow increases and intracellular glucose accumulation occurs until it reaches a limiting plateau. With a 10-fold Na^+ gradient, glucose accumulation ratios exceeding 100-fold can be attained without the need for any fixed stoichiometry, providing $\frac{L_{G-Na}}{L_G} = 1.1$. A 1,000-fold glucose accumulation gradient can be obtained with

$$\frac{L_{G-Na}}{L_G} > 1.1 \tag{52}$$

Glucose accumulation results in the energy gradient of glucose, X_G, becoming negative. This negative gradient acting via the reciprocal coupling reaction retards the rate of Na^+ entry, thus decreasing intracellular steady-state Na^+ concentration and thereby slightly increasing X_{Na} (Fig. 4i). When glucose inflow falls to zero at static head, although Na^+ influx slows, it does not fall to zero. This contrasts with the "ideal" behavior of the determinate model of cotransport (Fig. 4f–h).

An alternative static head exists for zero net Na^+ flux, when intracellular glucose is raised to a point where $-X_G$

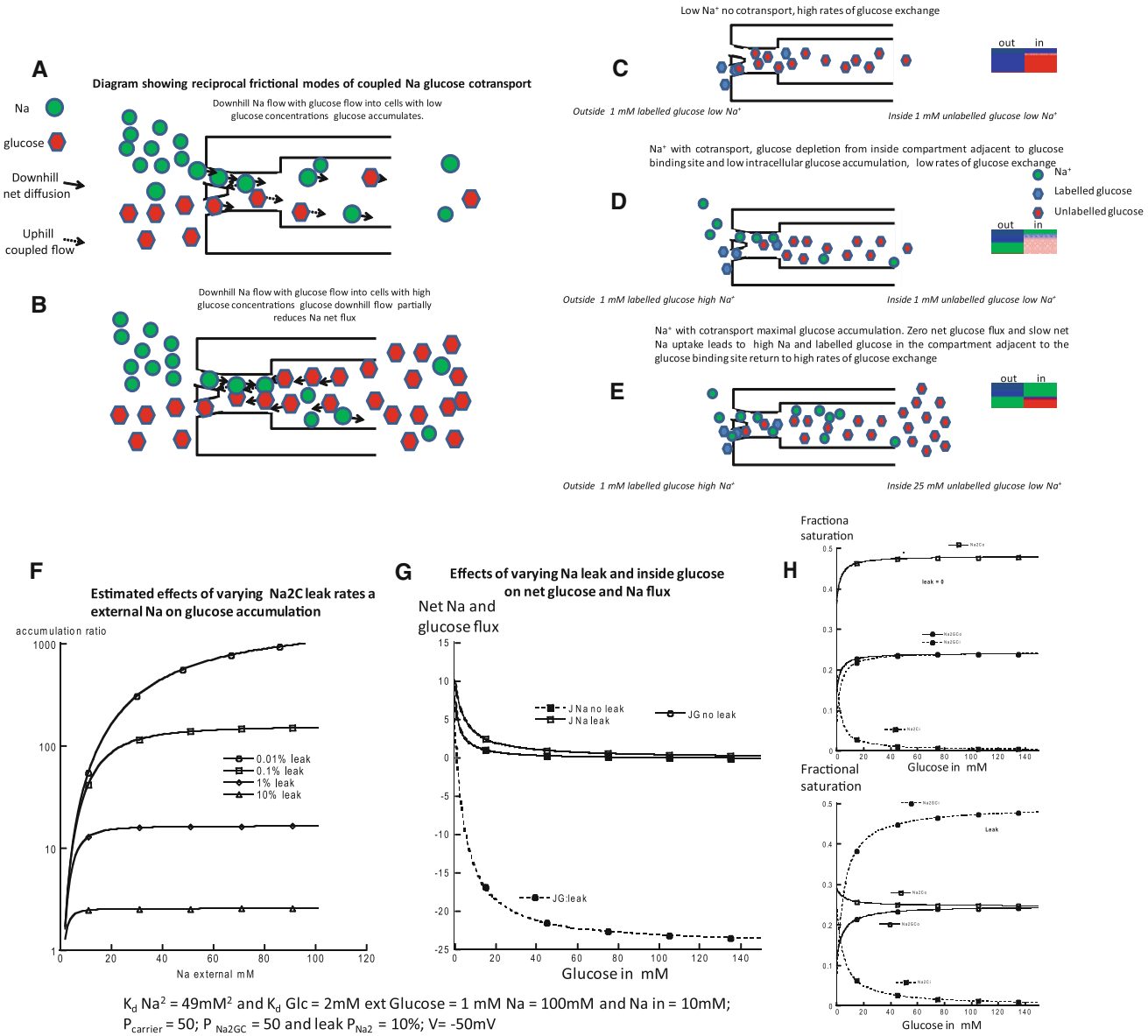

K_d Na^2 = 49mM^2 and K_d Glc = 2mM ext Glucose = 1 mM Na = 100mM and Na in = 10mM; $P_{carrier}$ = 50; P_{Na2GC} = 50 and leak P_{Na2} = 10%; V= -50mV

reduces $J_{Na} = 0$; although there is now zero net Na^+ flow, there is a backward leak flux of glucose.

$$G_{in}/G_{out} = \left(\frac{[Na]^{out}}{[Na]^{in}}\right) \cdot e^{\frac{L_{Na}}{L_{NaG}}} \quad (53)$$

This latter approach has been used (Chen et al. 1995) to show that the "stoichiometry" of Na^+ to α-methylglucoside (αMG) transport in isolated perfused *Xenopus* oocytes membranes overexpressing SGLT1 is close to 2. The observed relationship between the reversal potential of the Na^+ current and $Ln[\alpha MG]_{ext}$ was used to derive the stoichiometric coefficient (n). The failure of this relationship at low αMG concentrations was ascribed to an asymmetric inwardly rectifying Na^+ leak, which requires asymmetric rates of free carrier movement.

Incorporating the Mass Action Equations into the Formalism of Irreversible Thermodynamic Phenomenological Equations

A possible reason for the neglect of irreversible thermodynamics as a means of describing biological coupled flow processes is an influential and disparaging critique that Finkelstein published on the irreversible thermodynamic approach to osmosis (Essig and Caplan 1989; Finkelstein 1987). Finkelstein's authoritative, but erroneous, view together with its laudatory reception may have discouraged development of irreversible thermodynamic formalism for biological transport processes. Another reason why irreversible thermodynamics may not have been incorporated into biological transport formalism is that phenomenological

◀ **Fig. 4** **a** Diagrams of the frictional model of SGLT simulation of net Na^+–glucose coupled flows. Diagrams show separate portals for Na^+ and glucose at the external surface leading to a common "energy transduction friction chamber" where the ligands collide and a wider vestibule where the ligands collect prior to diffusion into the cytosol. **b** Na^+ concentrations are the same as in Fig. 5a, but intracellular glucose = 100 mM and extracellular glucose = 1 mM. The outwardly directed downhill glucose gradient interacts frictionally with Na^+ and tends to reverse the direction of net Na^+ flux in the transduction chamber, causing an increase in the endofacial Na^+ concentration, which thereby slows net Na entry and net glucose flux. **c** Na^+ is replaced by choline or K^+ and labeled glucose = 1 mM (*blue*) in the external solution and unlabeled glucose = 1 mM (*red*) in the inside solution. The model permits exchange flux at the glucose binding site on the external surface, represented here as overlapping red and blue spheres. Glucose-exchange flux is evident if glucose influx is slowed on removal of intracellular glucose. **d** Net Na^+ inflow from diffusion interacts with glucose in the "transduction chamber" to increase the force of inwardly directed glucose flow (*dotted arrows*), which leads to glucose accumulation within the cytosol and depletion within the vestibule and friction chamber. With an inwardly directed Na^+ gradient, Na outside = 140 mM, Na inside = 14 mM, external glucose = 1 mM and low intracellular glucose = 1 mM, there is friction generated between Na^+ inward flow and glucose which leads to a net inward glucose flux despite the lack of glucose concentration gradient. **e** When unlabeled glucose is present within the cytosol at high concentrations (25 mM) the unlabeled glucose attains sufficient concentration at the endofacial surface to restore high glucose exchange rates. **f** Conventional cotransport model predictions of the effects of varying Na^+ leak on net glucose and Na^+ flux, assuming a constant Na^+ gradient of 100 mM outside and 10 mM inside, a constant external glucose of 1 mM and variable cytosolic glucose from 0 to 150 mM. Na^2C leak is either 0% or 1% of the rate of vacant carrier C and Na^2GC carrier complex fluxes. The affinity parameters are symmetric. In the absence of Na_2 leak, both net glucose and Na^+ flux fall to zero when intracellular glucose = 100 mM. A small 1% Na^2C leak has a dramatic effect on net glucose flux, reducing the static head glucose from 100 to approximately 1 mM. This small Na^2C leakage increases net inward Na^+ flow to a small extent and reduces the retarding effect of raised intracellular glucose on Na^+ influx. The lines in **f** and **g** are all simulated using the symmetric cotransporter carrier model as simulated with Berkeley Madonna (v 8.314, www.berkeleymadonna.com). **g** *Central panel* shows the effects of varying intracellular glucose from 0 to 150 mM in the presence or absence of Na^+ leak on net glucose and Na^+ influxes and, in the *righthand panel*, the predicted changes in fractional saturation of the cotransporter substates Na^2C^o, Na^2C^i, Na^2GC^o and Na^2GC^i with or without a 1% Na^2C leak. The model predicts that raising intracellular glucose in the absence of Na leak will increase Na^2GC^o and Na^2GC^i to a similar extent, whereas with Na^2C leak Na^2GC^i is increased to a much larger extent than Na^2GC^o, hence accounting for the large decrease in glucose net uptake with small Na^2C leakage. Additionally, in the absence of Na^2C leak, raising intracellular glucose increases Na^2C^o but, with leak present, Na^2C^o decreases with raised intracellular glucose. **h** The predicted changes in Na^+ (*solid lines, open symbols*) and glucose net flux (*dotted lines, closed symbols*) on raising intracellular glucose from 0 to 160 mM and on altering the coupling coefficient from 0% to 29% of the Na^+ and glucose straight conductances with the frictional cotransport model are described diagrammatically in **a** and briefly in Eqs. 47 and 57. The simulations were produced using programs written in Berkeley Madonna. In the absence of coupling with Na^+, net glucose decreases to zero and then becomes negative as intracellular glucose is raised above 1 mM as seen with the conventional cotransport with Na^+ leak present. There is no effect of raising intracellular glucose on net Na^+ flux in the absence of coupling. Raising coupling coefficient L_{Na-G} above zero increases net glucose influx. Net uphill glucose flux is evident as the concentration required to reverse net glucose flux increases exponentially with L_{Na-G}. When L_{Na-G} = 29% of the straight conductances, the intracellular glucose concentration required to null glucose influx is > 100 mM. Increasing L_{Na-G} also reduces net Na^+ influx; however, with L_{Na-G} = 29% of L_{Na} when intracellular glucose is raised to 100 mM, an inward Na^+ leakage of approximately 30% of that observed in the absence of intracellular glucose is still present. **j** In this simulation glucose accumulates within the cytosol as a function of time, with intracellular Na^+ clamped at 14 mM, extracellular Na^+ = 140 mM and glucose = 1 mM. Intracellular glucose accumulates to a steady state. An exponential rise in steady-state glucose accumulation is observed when L_{Na-G} is increased between 25% and 30%. **k–m** Simulation of glucose equilibrium exchange fluxes in similar conditions to those shown in Fig. 5g, h; extracellular Na^+ = 140 mM, intracellular Na^+ = 14 mM, $L_{Na} = L_G$ = 1E-7 and L_{Na-G} = 2.5E-8. K_d values of Na^+ and glucose are the same as in Fig. 5h. The glucose-exchange permeability = L_{Gex} = 1E-8. Influx of sugar from the external solution is positive (*solid lines, open symbols*); efflux of glucose isotope from the inside is negative (*dotted lines, filled symbols*). The intracellular glucose isotope concentrations are held constant and at all times are equal to the external glucose concentrations, and it is assumed that during the time of observation no significant amount of glucose from the external solution accumulates within the cytosol. The key findings are that exchange efflux increases as intracellular Na^+ is raised, and this effect is exaggerated when the binding site is highly saturated. Similarly, exchange influx decreases as intracellular Na^+ is raised, and this effect is also amplified when the glucose binding site is close to saturation

Eqs. 47 and 57 are cast in terms of linearly coupled energy flows confined to the near-equilibrium condition that cannot be directly equated with saturable ligand binding interactions, using the law of mass action. However, since Peusner (1986) demonstrated that the Onsager relations extend beyond the near-equilibrium conditions, this constraint no longer applies. Conversion of mass flow to the equivalent energy flow permits the nonlinear ligand binding interactions terms which characterize conventional models of cotransport to be incorporated into the phenomenological equations. The net electrical force on cations $= \exp\left(\frac{-FV}{RT}\right)$, where F and V are the Faraday constant and potential difference experienced by the relevant cation, which can also be incorporated into X_i to generate an electrochemical force, as has been done with conventional models (Eskandari et al. 2005). Thus, the sequential stages of ligand movements across the various barriers within the transporter can be viewed as a linked sequence of phenomenological equations.

Equations 30 and 31 can be transformed from a description of mass flow to the equivalent energy flow as follows: The energy gradient driving Na^+ flow, X_{Na}, between the external solution and the binding site, where X_{Na} is the nonlinear force (joules cm^{-2}) determining steady-state Na^+ distribution between the external solution and its neighboring binding site at the external surface of the transporter is

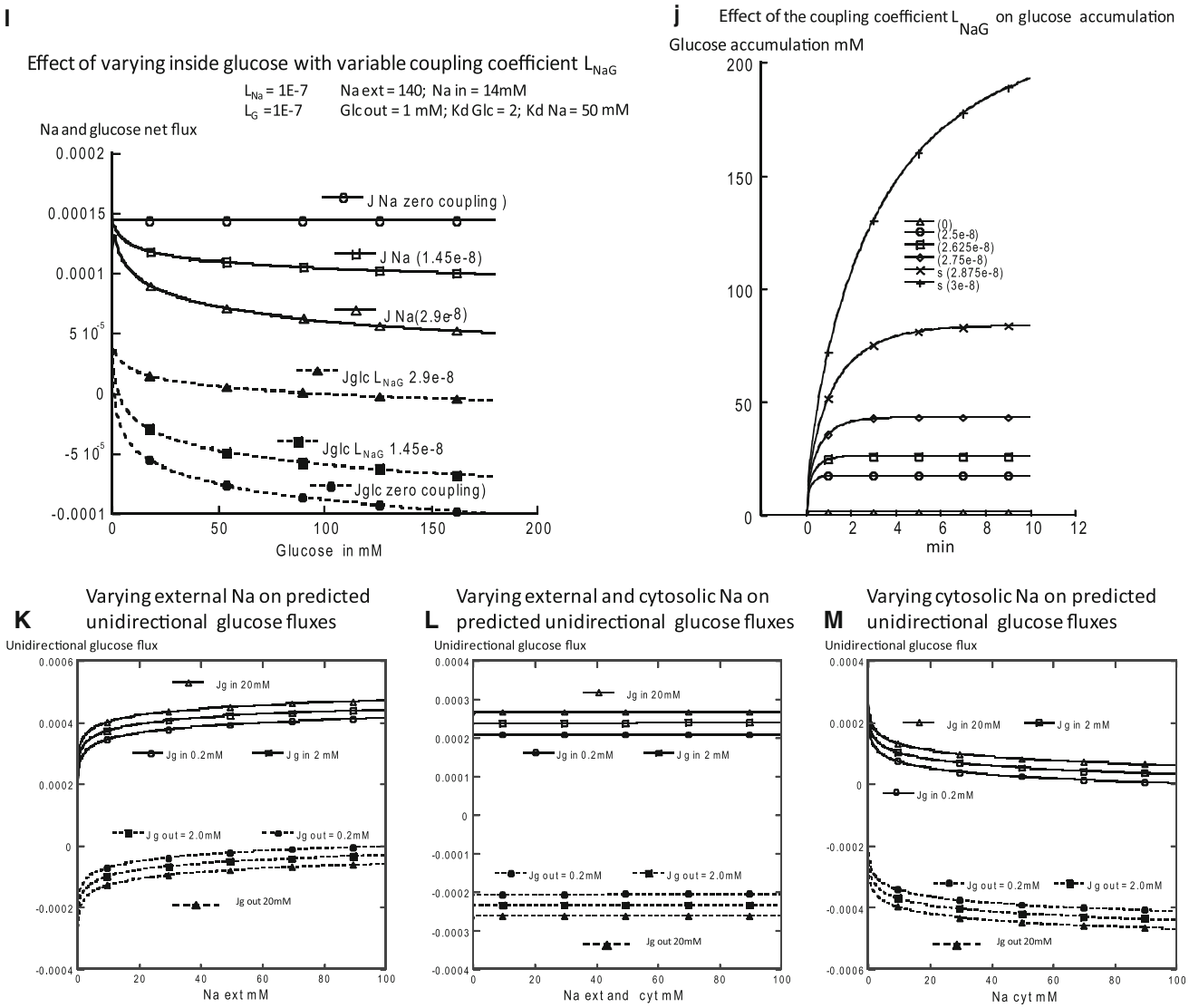

Fig. 4 continued

$$X_{Na} = RTLn\left(\frac{\text{Forward Na flux}}{\text{reverse Na flux}}\right) = RTLn\frac{\left([Na]^{out}\cdot C^{out}\right)}{\left(NaC^{out}\cdot K^{out}_{D_{Na}}\right)} \tag{54}$$

The equation for Na^+ flow between the external solution and the external binding site, J_{Na}, can be recast as follows:

$$L_{Na}\cdot RTLn\frac{\left([Na]^{out}\cdot C^{out}\right)}{\left(NaC^{out}\cdot K^{out}_{D_{Na}}\right)} = L_{Na}\cdot X_{Na} \tag{55}$$

L_{Na} remains the rate coefficient relating the Na^+ energy flow between the external solution and initially its external binding site (mole joule^{-1} s^{-1} area^{-1}). Similarly, the energy gradient for Na^+ flow from the binding site to solution in the central cavity is

$$RTLn\frac{\left(NaC^{out}\cdot K^{out}_{D_{Na}}\right)}{\left([Na]^{inter}\cdot C^{out}\right)} \tag{56}$$

Frictional Models of Coupled Sodium–Glucose Transport and Coupled Sodium, Chloride and Dopamine Transport

To simulate biological coupled flow processes, the flow-induced coupling forces between mobile ligands are modeled as a serial stages between adjacent compartments. Saturable transport and cotransport processes at the outer surface of the transporter involve independent reversible binding of Na^+ and glucose to and from their separate

selectivity sites. This is followed by permeation of ligands with coupled interactions through the narrow transducing central channel segment traversing the transporter. The frictional models illustrated in Figs. 4a–e, 5a and 6b assume separate ligand binding sites in the occluding zone of SGLT, or the DAT.

A clear separation between ligand binding and transport rates has been observed in the DAT, with binding rates being faster by two orders of magnitude than those for transport (Schwartz et al. 2003; Schwartz et al. 2005). Thus, initial ligand binding and selectivity can be viewed as separate processes from transport and cotransport. The binding sites act as saturable selective entry ports that, in the case of SGLT, funnel Na^+ and glucose or, with DAT, funnel Na^+, Cl^-, K^+ and DA from the external solution into the central cavity traversing these transporters. No competitive ligand interactions are required between Na^+ and glucose at their separate sites. Net transport of both Na^+ and glucose between the external solution and central compartment depends entirely on the forces generated by their local concentration (energy) gradients between each stage of the overall transport process. However, in non-equilibrium conditions, where net ligand flows occur, these forces can alter the local ligand concentrations at the exo- and endofacial surfaces of the entry sites and affect the "operational" kinetic parameters for transport (K_m and V_m) across the transporter ensemble. Thus, glucose depletion from the endofacial layer adjacent to the glucose selectivity site, generated by frictional interactions of glucose with net Na^+ inflow, will reduce the apparent affinity for glucose and create asymmetries in the cotransport parameters.

Since exchanging glucose isotopes in SGLT transport or exchanging neurotransmitter isotopes bind to the same site in DAT and SERT and engage in accelerated exchange transport, they are assumed to behave competitively with each other, as already described for exchange in GLUTs in Eqs. 26 and 27. In the distal part of the confluent permeation pathway glucose in SGLT (Fig. 4c–e) or DA in DAT (Fig. 5a) undergoes frictional interactions with the driving ligand Na^+, which lead to local changes in glucose or DA in SGLT or DAT, respectively, which change local and, hence, net flow rates. Beyond the coupling zone both glucose and Na^+ ligands in SGLT or Na^+, Cl^- and DA in DAT diffuse independently without significant frictional interactions through the wider part of the common central pathway to the cytosolic pool.

Neurotransmitter coupling via DAT, in addition to exchange between DA and AMPH, involves flow of Na^+, K^+ and Cl^- and can be viewed as the resultant of both direct and indirect couplings occurring within the restricted confines of the friction transduction chamber. These interactions can be simply represented as an Onsager matrix.

$$\begin{aligned}
J_{Na} &= L_{Na-DA}\cdot X_{DA} + L_{Na}\cdot X_{Na} + L_{Na-K}\cdot X_K \\
&\quad + L_{Na-Cl}\cdot X_{Cl} + L_{Na-AMPH}\cdot X_{AMPH} \\
J_K &= L_{K-DA}\cdot X_{DA} + L_{K-Na}\cdot X_{Na} + L_K\cdot X_K \\
&\quad + L_{K-Cl}\cdot X_{Cl} + L_{K-AMPH}\cdot X_{AMPH} \\
J_{Cl} &= L_{Cl-DA}\cdot X_{DA} + L_{Cl-Na}\cdot X_{Na} \\
&\quad + L_{Cl-K}\cdot X_K + L_{Cl}\cdot X_{Cl} + L_{Cl-AMPH}\cdot X_{AMPH} \\
J_{DA} &= L_{DA}\cdot X_{DA} + L_{DA-Na}\cdot X_{Na} + L_{DA-K}X_K\cdot \\
&\quad + L_{DA-Cl}\cdot X_{Cl} + L_{DA-AMPH}\cdot X_{AMPH} \\
J_{AMPH} &= L_{AMPH-DA}\cdot X_{DA} + L_{AMPH-Na}\cdot X_{Na} + L_{AMPH-K} \\
&\quad \cdot X_K + L_{AMPH-Cl}\cdot X_{Cl} + L_{AMPH}\cdot X_{AMPH}
\end{aligned} \tag{57}$$

where J_{Na}, J_K, J_{Cl}, J_{DA} and J_{AMPH} are the fluxes (moles cm^{-2} s^{-1}) of Na^+, K^+, Cl^- and DA^+; $AMPH^+$ are the isotopic neurotransmitter exchanging ligands; and X_i (joules cm^{-2}), as before, is the energy gradient, e.g., $X_k = RTLn\,(K^o/K^i)$. In all cases the coupling coefficients obey the Onsager relationship, i.e., $L_{ij} = L_{ji}$; hence, $L_{K-DA} = L_{DA-K}$, etc., where L is the conductance (J $mole^{-1}$ cm^{-2} s^{-1}).

The matrix description of DA/AMPH cotransport (Eq. 57) and the simpler frictional model of SGLT (Eq. 47) have important advantages over the conventional models of cotransport, not least because the various possible combinations of coupling interactions are easily and unambiguously represented and programmable within simulation algorithms.

Coupling between K^+ and/or Cl^- and neurotransmitter may be indirect, via K^+–Na^+ or Cl–Na^+ coupled interactions, rather than direct, via coupling between K^+ or Cl^- and the neurotransmitter. With coupling between DA, Na^+ and K^+, if the coupling coefficient $L_{K-DA} = 0$ but $L_{Na-K} = -0.1$ and $L_{DA-Na} = 0.1$, even although no direct coupling interaction between K^+ and DA^+ exists, an indirect coupling reaction will occur because K^+ and Na^+ fluxes are negatively coupled and Na^+ flux is coupled with DA. Thus, an outward gradient of K^+ will increase the force of inward Na^+ movement (Fig. 5j); and since Na^+ and DA^+ fluxes are directly coupled, the force of K^+ gradient coupling on Na^+ flux will indirectly increase the force of the directly coupled Na^+-dependent DA^+ flow. Although requiring that Na^+ be present, the K^+-activated DA flux does not require an Na^+ gradient to drive uphill flow of DA since the indirect coupling force is generated entirely by the K^+ gradient acting on the force on Na^+, which then interacts with DA. Similarly, direct coupling of Cl^- inflow to Na^+ inflow can enhance the direct coupling between Na^+ and neurotransmitter, permitting exchange fluxes without any direct interactions between Cl^- and neurotransmitter being required. These kinds of indirect interaction could explain some of the anomalous partial

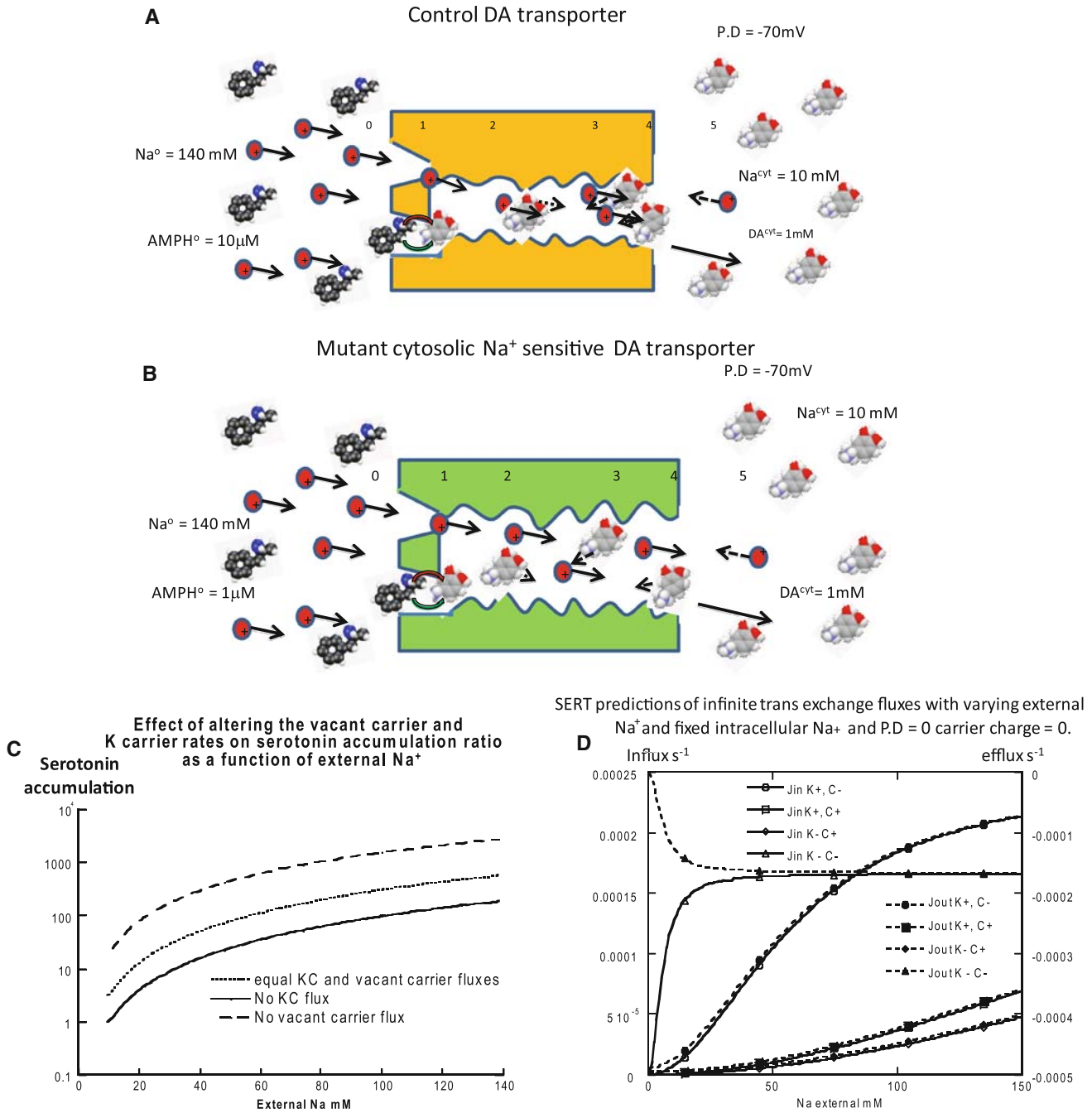

dependencies of 5-HT or DA accumulation on Cl^- and K^+ (Erreger et al. 2008; Nelson and Rudnick 1979; Zomot et al. 2007).

Friction Chamber Interactions with Exchange

In conditions where there are high rates of net glucose or neurotransmitter inflow, with near to equimolar isotopic glucose or DA present in the inside solutions, i.e., where the driving force for either net glucose or neurotransmitter flow X_{Glc} or $X_{DA} = 0$, frictional coupling with Na^+ depletes labeled glucose or labeled neurotransmitter from the endofacial solution immediately adjacent to binding site (Figs. 4d, 5a). This reduces isotope exchange flux because it depends on the presence of the exchanging isotopes on the opposing sides, as was shown with glucose exchange via GLUTs (Baker and Widdas 1973) and the fixed asymmetric site models (Cloherty et al. 1996; Leitch and Carruthers 2009; Naftalin 2008a; Naftalin et al. 1985).

The simulations of Na^+–glucose or Na^+–neurotransmitter cotransport with the stochastic coupling models show that when intracellular glucose or neurotransmitter

◀**Fig. 5** **a** Diagrams showing the salient elements of the frictional model for Na^+-dependent DA transport and accumulation. *Upper panel* shows the elements of the DAT in control mode. The segments of the system are numbered 0–5. The external solution and internal solution are labeled 0 and 5, respectively. Amphetamine (AMPH) is present at 10 μM in the external solution along with 140 mM Na^+. In segment 1 the external vestibule of DAT is diagrammed, showing separate portals for Na^+ and neurotransmitter uptake. The portal for AMPH permits both net and exchange, represented by *curved arrows*, with DA present in the inner solution and inner layers of the transporter at this site. In segment 2 the narrow common central channel is shown, in which net diffusive flux is represented by *straight unbroken arrows*; *broken arrows* represent convective flux generated by friction and diffusion resulting from enforced proximity of ligands in the narrow channel of the friction chamber. Segments 3 and 4 represent the endofacial segments of the central channel, where a second narrowing, if present, can act as an additional low-affinity exchange site. This second site is not essential to demonstrate the frictional model, so it is not implemented with DAT or SGLT simulations. The direction of the arrows indicates that Na^+ is flowing down its electrochemical potential gradient into the low Na^+ and negative electrical potential cytosolic solution, whereas accumulated DA is present at 1 mM in the inside solution segment 0, flows downhill toward the external solution and in so doing reduces the force of Na^+ inward diffusion. **b** *Lower panel* shows a mutant form of DAT in which the central channel is slightly wider than in the wild-type transporter in the *upper panel*. The frictional interactions between DA and Na^+ in the central channel are now absent; this permits DA to accumulate in segment 1 to a much higher concentration and thereby stimulate exchange with AMPH. **c** Simulations with the conventional SERT $2Na^+$:1 Sert symport:1 K^+ antiport predicting steady-state 5-HT accumulation with extracellular $Na^+ = 140$, $K = 5$ mM and $K^+ = 140$ mM; extracellular 5-HT = 1 μM; and extracellular Na^+ varied from 0 to 140 mM. Affinities are assigned to be symmetric, $K_{DNa2} = 50$ mM, $K_{DK} = 5$ mM and $K_{D5\text{-}HT} = 0.1$ μM. The rates of carrier–K^+ complex equilibration = rates of Na_2:S carrier complex equilibration = 100 s^{-1}; the rate of vacant carrier equilibration = 0 or 100 s^{-1}. The accumulation ratio 5-HT = intracellular/extracellular. The model demonstrates that the outward K^+ gradient increases steady-state 5-HT accumulation by 10-fold at any inward Na^+ gradient where the mobility of the vacant carrier reduces the maximal accumulation possible at any given Na gradient. The simulations are produced using programs written in Berkeley Madonna. **d** Predicted infinite *trans* unidirectional fluxes of the SERT carrier with 1 μM 5-HT labeled in the external solution and 1 mM in the cytosol as a function of changing external Na^+ with constant cytosolic $Na^+ = 14$ mM and constant K^+ inside and outside as in **c**. The highest influx and efflux are obtained with the rates of K^+–carrier and Na_2S–carrier complex = 100 and vacant carrier flux = 0 (K^+, C^-) than with vacant carrier flux = 100 at high extracellular Na (K^+, C^+). However, high rates of exchange with the model are obtained when both vacant carrier and K-carrier complexes are absent (K^-, C^-); in this condition exchange rises from zero at external $Na^+ = 0$ mM to a maximum at around 50 mM Na^+. **e** The conventional SERT $2Na^+$:1 SERT symport:1 K^+ antiport predicts steady-state 5-HT accumulation as a function of membrane potential. The rates of carrier–K^+ complex equilibration = rates of Na_2:Sert carrier complex equilibration = 100 s^{-1}; the rate of vacant carrier equilibration = 0 or 10 s^{-1}. The accumulation ratio 5-HT = intracellular/extracellular. The carrier and its complex are assumed to carry a charge, z, which can be assigned values of –2 to 0. Thus, the net charge of the Na_2:Sert carrier form with $z = -2 = +1$. Steady-state accumulation is bell-shaped with respect to transmembrane potential, with optimal accumulation observed between –25 and 0 mV. The more negative charge forms have more accumulation optima at more negative potentials. The major difference between SERT and SGLT is the extent of accumulation, 3.5×10^4-fold with zero vacant carrier movement and 2.3×10^4 with vacant carrier mobility 10% of Na_2GC mobility, respectively. Reducing carrier charge from –2 to zero reduced the optimal accumulation by sevenfold. The maximal accumulation ratio falls steeply at positive potentials. The decline in accumulation is steeper with more negatively charged carrier. **f** An explanation for the predicted bell-shaped relationship between accumulation and membrane potential is that the distribution of carrier complex SNa_2Co decreases and SNa_2Ci falls as a sigmoid function of potential. The steepness of this rise and fall with membrane potential varies inversely on the carrier charge. **g** Simulations of a frictional model of Na–K-Cl–serotonin cotransport using Eq. 57. Effect of altering external Na and the coupling coefficient L_{NaS} on net Na influx and serotonin static head accumulation. Net Na influx increases as a hyperbolic function of Na external concentration. Na^+ influx is increased on raising the coupling coefficient L_{NaS} above zero with a low intracellular serotonin concentration (*unbroken lines*). When $L_{NaS} = 0$, increasing external Na^+ has no effect on serotonin accumulation; when $L_{NaS/LNa} = 0.5$, serotonin accumulates by 100-fold with a 10-fold Na gradient. **h** 5-HT accumulation is frictionally coupled to Na^+ influx and displayed as a function of transmembrane potential and the frictional coefficient L_{NaS}. *Lowest line* shows 5-HT accumulation in the absence of Na^+ coupling as a passive function of membrane potential. At –120 mV 5-HT with a single positive charge is passively accumulated by 100-fold as a result of the negative electrochemical potential. Increasing the membrane potential to +50 mV reduces passive 5-HT accumulation by 1,000-fold. When a coupling coefficient between Na^+ and 5-HT flux of 1.25E-6 is present, steady-state 5-HT accumulation is approximately 10^5-fold between –80 and –120 mV and decreases to 10-fold at zero PD. Raising the coupling coefficient to its limit of 2.5E-6 increases the 5-HT accumulation to over 10^6 in the range between –120 and 50 mV. **i** The equilibrium exchange unidirectional serotonin fluxes as a function of varying external Na^+ at zero transmembrane potential with external and internal serotonin concentrations = 1 μM. When $L_{NaS} = 0$, varying external Na^+ has no effect on either influx or efflux. Raising L_{NaS} results in an Na^+-dependent increase in exchange influx and a reciprocal decrease in efflux. **j** The effects of varying the coupling between Na^+ and K^+ from 0 to –5E-7 on Na^+-dependent 5-HT accumulation and Na^+ influx at varying external Na^+ and a fixed coupling coefficient between 5-HT and Na^+ $L_{NaS} = 6E\text{-}6$ mol joule^{-1} cm^{-2} s^{-1}. In the absence of external Na^+, Na^+–K^+ coupling has no effect on 5-HT accumulation. However, as the Na^+ gradient is increased, Na^+–K^+ coupling enhances Na^+ gradient–dependent 5-HT accumulation. A negative coupling coefficient enhances the rate of Na^+ influx when there is an outwardly directly K^+ gradient. **k** Simulation of the effects of reducing either external Na^+ (*broken lines*) or Cl^- (*continuous lines, open symbols*) from 140 to 5 mM on AMPH DA exchange efflux as observed by Pifl and Singer (1999) in superfused human embryonic kidney cells stably transfected with DAT cDNA. The nonmetabolizable DA analogue [^{3}H] 1-methyl-4 phenylpyridinium (4-MPP) was used to monitor exchange efflux across DAT. AMPH was observed generate more exchange efflux than unlabeled DA. These results differ from the conventional model, which predicts a zero or minimal response to altered external ion concentration on DA efflux. In contrast, the frictional model predicts that reducing the Na^+ gradient or Cl^- gradient will reduce coupled inflow and, hence, increase efflux. It seems likely that there is coupling between Na^+ and Cl^- influx; hence, reducing external Cl^- from 140 to 5 mM has a smaller effect on DA efflux than a similar reduction in Na^+. Model variables and parameters: Na inside = 30 mM, Cl inside = 27 mM, $K_{DNa} = 10$ mM, $K_{DCl} = 100$ mM, $K_{DDA} = 3.5$ μM, DA inside = 3 mM, AMPH external = 10 μM, $K_{DAMPH} = 0.26$ μM, $L_{Cl} = 2.0E\text{-}7$ mM, $L_{Na} = 3.8E\text{-}8$ mM, $L_{DA} = 1.E\text{-}10$ mM, $L_{NaCl} = 3.7E\text{-}9$ mM, $L_{NaS} = 6.2E\text{-}10$ mM, L_{DA}

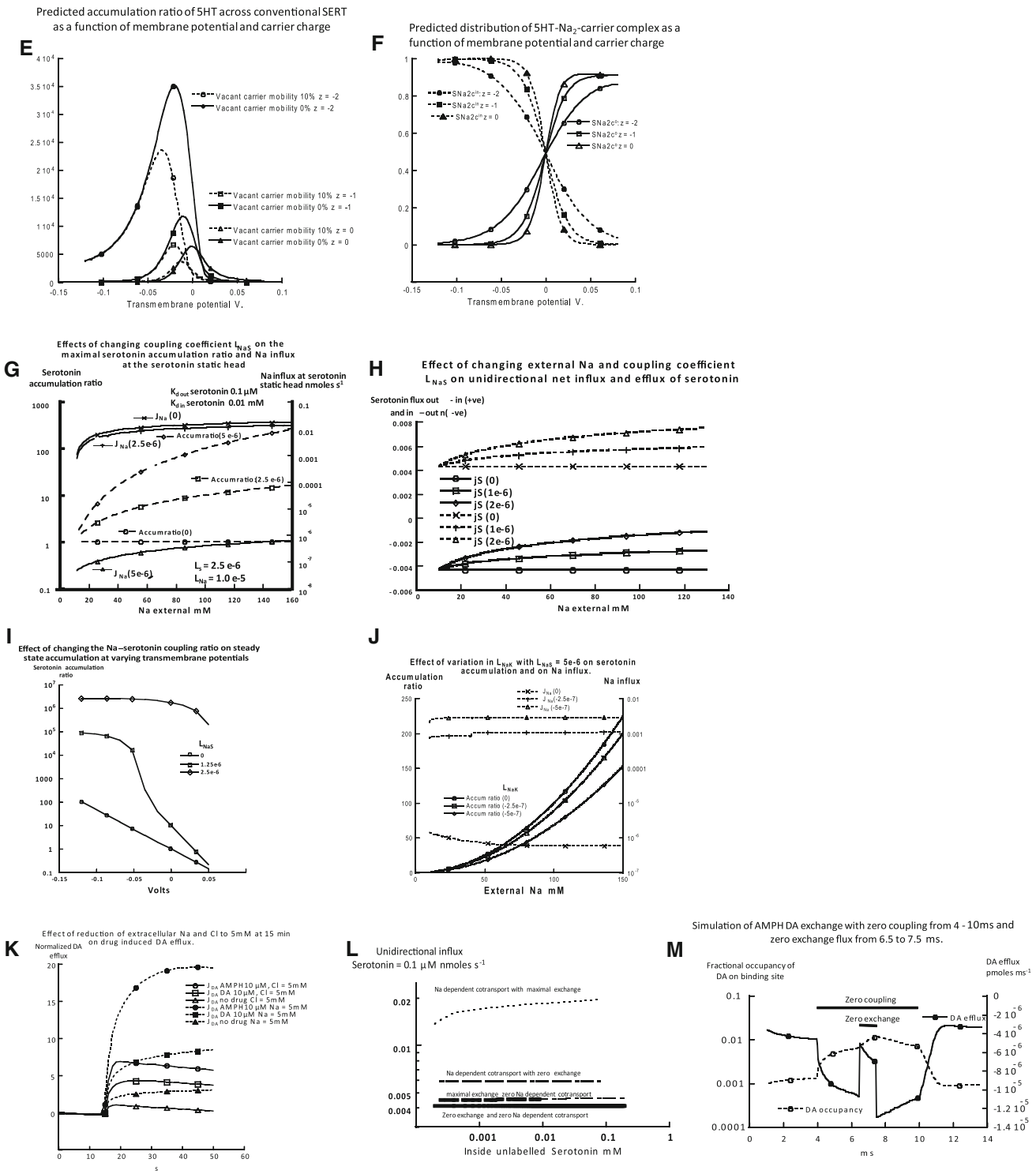

Fig. 5 continued

accumulation reaches the upper limit to which it can be driven by the force available from coupled Na^+ and other ligand interactions, back-diffusion from the cytosolic solution will replete the endofacial layer of glucose or neurotransmitter and net glucose or neurotransmitter influx will fall to zero because the ligand concentrations on both sides of the transporter will be equalized. This is illustrated in cartoon form in Fig. 4e and simulated in Figs. 4k–m for Na^+–glucose cotransport via SGLT and serotonin cotransport via SERT (Fig. 5g, l).

◀ **Fig. 5** continued

exchange = 1.0E-10 mM and L_{AMPH} = 3.0E-11 units of L = mole joule^{-1} cm^{-2} s^{-1}. **l** The extent of infinite *trans*-exchange influx of serotonin from a fixed external concentration into cells containing varying unlabeled serotonin concentrations is determined both by cotransport and the exchange coefficient. In the absence of any accelerated exchange, serotonin influx is unaffected by intracellular serotonin. When the exchange coefficient L_{Sex} = 1E-7, with L_S = 1E-6 as in **g** and **h**, exchange influx is increased. Exchange influx is only marginally affected by altered intracellular serotonin in the absence of cotransport. When cotransport is present (L_{NaS} = 2E-6), as in Fig. 5g, raising intracellular serotonin raises serotonin influx. **m** Simulation of dual modes of AMPH DA exchange as observed by Kahlig et al. (2005). The frictional model simulates the rapid interchange between the dual modes of exchange DA exchange efflux by reversible switching on and off of the coupling interactions between all the ligands, namely, Na^+ Cl^-, DA and AMPH. Thus, during the period of zero coupling at 4–10 ms, the coupling coefficients are all reduced to zero. The straight diffusion coefficients are unaltered, as are the exchange rates. To demonstrate the role of exchange, external AMPH is removed from 6.5 to 7.5 ms; thus, exchange efflux of DA is no longer present during this period. The effect of uncoupling is to increase DA exchange efflux. This increase is due entirely to enhanced DA binding to the exchange site because the "sweeping away" effect of the coupled interactions is temporarily diminished, so more DA from the inside solution can approach the binding site and exchange with external AMPH. Model variables and parameters: Na external = 140 mM, Cl external = 140 mM, Na inside = 14 mM, Cl inside = 14 mM, DA inside = 10 mM, AMPH external = 0.1 μM, $K_{DNa\ external}$ = 25 mM, K_{DCl} = 10 mM, K_{DDA} = 5 μM, K_{DAMPH} = 0.3 μM, L_{Na} = 2e-8 mM, L_{Cl} = 1e-7 mM, L_{DA} = 5e-10 mM, L_{AMPH} = 1e-11 mM, $L_{Na\text{-}DA}$ = 5e-9 mM, $L_{Na\text{-}Cl}$ = 1e-8 mM and L_{DA} exchange = 5e-10 L = moles joule^{-1} cm^{-2} s^{-1}

If in this steady-state condition with zero net glucose or neurotransmitter flux, the unlabeled external glucose or neurotransmitter is replaced with equimolar labeled ligand, then high rates of exchange flux are observed. These high rates are similar to those observed without Na^+ present and with high concentrations of exchanging ligand on both sides of the membrane. These phenomena have been observed experimentally with glucose exchanges via SGLT when the Na^+ gradient is removed either by reduction of extracellular Na^+ or by raising intracellular Na^+ toward the extracellular Na^+ concentration (Centelles et al. 1991; see below).

Unidirectional Ligand Fluxes via the Conventional SGLT, SERT or DAT Models

The most sensitive way of discriminating between contending cotransport models is by comparing their predictions of unidirectional flux variation in relation to *cis* and *trans* concentrations of Na^+ or membrane potential. Alternating cotransport models with stoichiometric coupling between glucose and Na^+ predict that raising cytosolic Na^+ should not alter unidirectional Na^+ inflow greatly but substantially raise exit flux.

Experimental Observations of Glucose Exchanges via Na^+–Glucose Cotransporter

Labeled glucose-exchange fluxes across isolated pig kidney brush-border membrane vesicles showed an Na^+-dependent increase in zero-*trans* glucose net influx on raising external Na^+ from 0 to 10 mM but a decrease in equilibrium exchange influx (Centelles et al. 1991). The decreased unidirectional glucose-exchange flux is inconsistent with the conventional cotransport model but is predicted by the friction model (Fig. 4a–e). Unidirectional glucose influx was stimulated by high intravesicular glucose (20 mM), and an outward Na^+ gradient increased both unidirectional glucose exit flux and exchange flux.

Raising intracellular Na^+ inhibited Na^+-dependent glucose influx at zero membrane potential, termed the "*trans* inhibition effect" of Na^+. This effect was alleviated by an inside negative potential. Conversely, reducing extracellular Na^+ increases glucose efflux (Kessler and Semenza 1983; Semenza et al. 1984, 1985). These findings were rationalized by proposing that the vacant carrier has a large natural asymmetry in the absence of a membrane potential, with inward rates exceeding outward rates by 10-fold. A negative charge on the carrier permits the membrane potential to alter distributions of mobile carrier and ligand carrier complexes. When the vacant carrier had a charge (z) of 0, Na^+-dependent *trans* inhibition decreased membrane potential and was made more negative. When carrier charge = –1, increasing the inside negative potential reduces Na^+-dependent *trans* inhibition.

A similar phenomenon using estimates of bidirectional fluxes of D-galactose and α-methyl-D-glucose across sheets of isolated rabbit ileal mucosa mounted in flux chambers showed that increasing extracellular Na^+ from 0 to 140 mM increased unidirectional galactose influx (2 mM) across rabbit intestinal brush-border membrane from the mucosal solution to cytosol by 15-fold but the retarded cell to mucosal flux by 10-fold. Ouabain pretreatment reduced the Na^+-dependent mucosal to cell influx and increased cell to mucosal efflux (Holman and Naftalin 1975, 1976; Naftalin and Holman 1974). These latter findings were explained by friction-driven convective coupling between Na^+ and glucose movements, which retards efflux of the upstream labeled ligand flow while enhancing influx.

The contrasting predictions of the simulations of conventional SGLT alternating carrier and the friction-driven cotransporter on Na^+-dependent unidirectional glucose fluxes are shown in Fig. 4g, h and in Fig. 4k, m, respectively. The conventional alternating model predicts no alterations in either Na^+-dependent glucose influx or efflux when the *trans* Na^+ concentration is altered, whereas the frictional model predicts that an increase in the coupling

A **The relative positions between the key amino acids which are the sites of the external, central and internal Cl^- binding sites.**

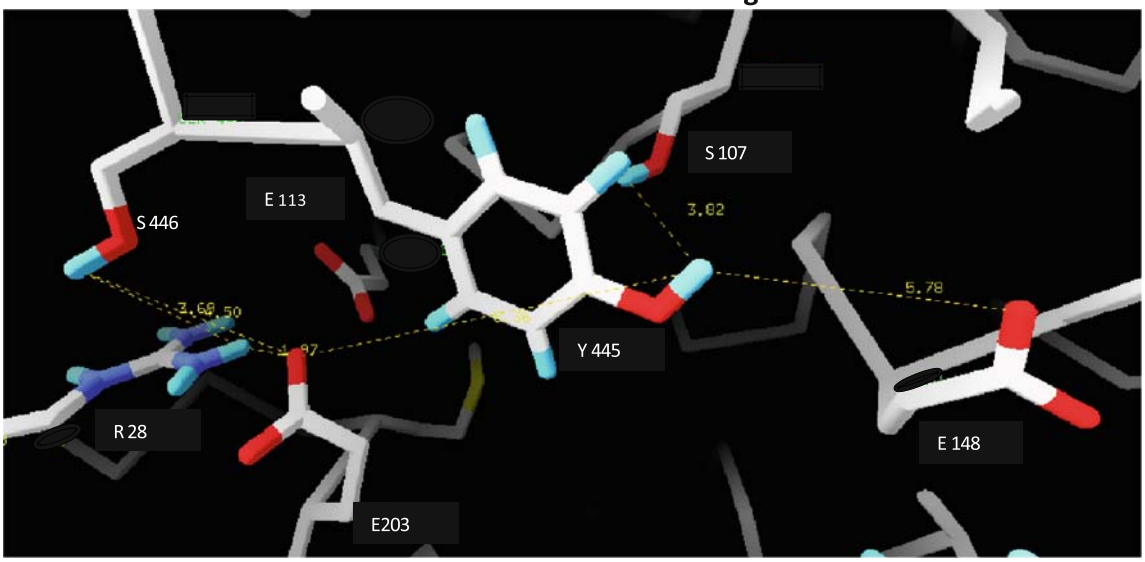

B **Diagram showing a structural model for Cl^-/H^+ exchange/ cotransport in ClC channel .**

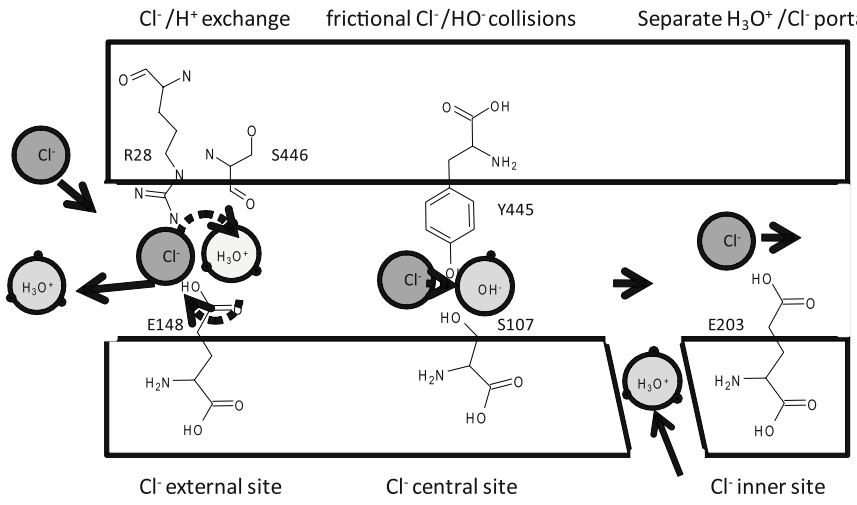

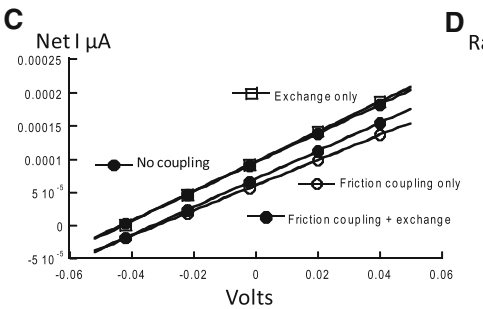

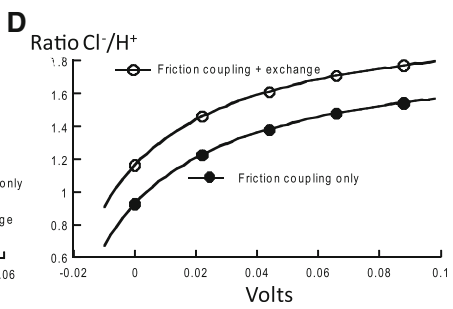

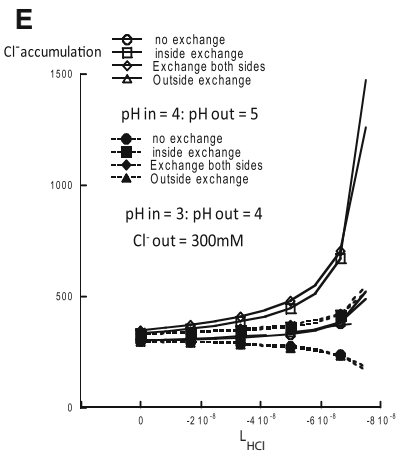

Cl in = 45, Cl out = 300; H in= H out = 1mM; K_{DH}= 1E-5 M; K_{DCl} = 100mM L_{HCl} = -3.5E-8;exchange= 2E-9; L_{Cl} = 1E-7;L_H = 1E-8;

◀ **Fig. 6** **a** The central channel within the Cl transporter taken from the coordinates posted in Protein Data Bank under codes 10TS, 10TT and 10TU and published in Dutzler et al. (2003). The distances between the external Cl binding site at the Glu-148, Arg-28 and Ser-446 residues and the central Cl binding site between the hydroxyl residues of Ser-107 and Tyr-445 and the internal site at Glu-203 are shown. **b** Part a is used as a basis for the frictional model of Cl^-, H^+ and OH^- interaction within the CLC channel. The region between R28 guanidyl and E203 carboxyl residues could permit simultaneous Cl^- and H^+ binding and exchange. The narrow passage width between the S 107 and Y445 OH groups is a potential region of friction between Cl^- and OH^- anions, and it is possible that Cl^- and protons can enter and leave at the inner end of the channel by separate paths. **c–e** Simulations of Cl^- H^+ fluxes as a function of transmembrane potential (Accardi et al., 2004; Accardi and Miller, 2004) with external Cl^- mM, internal Cl^- = 300 mM and H^+ external = H^+ internal = 0.1 μM. The estimated total net current is displayed as a function of transmembrane potential in **c**. The Nernst potential for the outward Cl^- gradient is –43 mV, close to the ideal value of 49 mV in a perfectly Cl^-selective membrane. With negative coupling between Cl^-:H^+ L_{HCl} = –3.5E-8, the null potential is shifted to –33 mV; implementing Cl^-:H^+ exchange at either the external or internal site or both sites has only a minor effect on the null potential, $L_{exchange}$ = 2E-9. However, the predicted flux ratio of Cl^-:H^+ at all positive potentials in the range 0–100 mV increases from a ratio of around 1:1 at 0 mV to 1.6-1.8:1 at 100 mV. **d** The frictional models of Cl–H interaction and exchange are similar to those described for SGLT (Fig. 5a–h) and are simulated with Berkeley Madonna as before. **e** A static pH gradient of 1 unit directed either outwardly or inwardly generates Cl^- accumulation for an outwardly directed gradient or Cl^- depletion for an inwardly directed similar to the experimental observations (Accardi et al. 2004; Accardi and Miller 2004). With an outward H^+ gradient Cl^- accumulates as an exponential function of $-L_{HCl}$, reaching a limit of approximately 10-fold with L_{HCl} = –8.2E-8. It is observed that the exchange coupling has an asymmetric effect on Cl^- accumulation. Implementation of Cl:H exchange on the inside of the transporter has a negligible effect on Cl^- accumulation, whereas when the exchange function is present either on both sides or on the outside only, Cl^- accumulation is almost abolished. L_{HCl} exchange = 2E-9 as in **c** and **d**. **f** Either an outward or an inward Cl gradient of 300:45 mM simulates the results of Accardi et al. (2004) and Accardi and Miller (2004). With no exchange or frictional interaction, the inside and outside pH values are the same (= 5). Decreasing L_{HCL} from 0 to –5E-8 causes a 2.5-fold pH decrease or increase with an outwardly directed or inwardly directed Cl gradient, respectively. Implementation of the exchange function alters coupled pH asymmetrically. Implementation of exchange solely on the outside is without effect on Cl^- gradient–dependent proton accumulation or depletion. However, when exchange is implemented at the inside of the transporter, it reduces intracellular pH by two units at all levels of frictional coupling. **g**, **h**The bimodal nature of Cl conductance activity as observed by Alekov and Fahlke (2009) is demonstrated here by temporary uncoupling of the frictional coefficient, L_{HCl}. These panels demonstrate the effects of short-term uncoupling of the frictional interactions between Cl^-:H^+ with an inwardly directed Cl^- gradient of 300:45 mM and no pH gradient (pH = 3). A step increase in current is observed from 5 to 5.2 μS at –80 mV, when the coupling coefficient changes from 3E-8 to 0. This is caused by reciprocal changes in the fractional saturations of Cl^- and H^+ at the external Cl/H binding site as the "sweeping away" effect by the frictional interaction is temporarily halted

coefficient between Na^+ and glucose results in an Na^+ gradient–dependent increase in glucose influx and decrease in efflux during isotope exchange. The alternating cotransport model also predicts that glucose influx will be absent when Na^+ is absent from the external solution. Any glucose flux observed in these conditions would require a glucose leak pathway, which is unassigned in the conventional models of glucose cotransport (Eskandari et al. 2005; Semenza et al. 1985; Turner 1981). Additionally, conventional alternating models predict that with equal Na^+ concentrations in inside and outside solutions, unidirectional influx and efflux should increase equally as hyperbolic functions of the Na^+ concentrations. However, abolishing Na^+ gradients with ouabain abolishes both the Na^+-dependent increases and decreases in glucose influx and efflux across the brush border and brush-border membrane vesicles, contrary to the predictions of the conventional alternating carrier model for SGLT or SERT (Figs. 4h, 5d) (Kessler and Semenza 1983; Naftalin and Holman 1974; Semenza et al. 1984, 1985).

Exchanges with 5-HT and DA Cotransport

Neurotransmitter transporters tend to accumulate their ligands into vesicles or neuronal cytosol, where the steady-state accumulations are close to the tipping point of the transporters. Thus, small changes in intracellular Na^+ or Cl^- or membrane potential can reverse the direction of net neurotransmitter flow. Neurotransmitter efflux followed by accumulative reuptake causes large and very rapid alterations in neurotransmitter concentration inside the narrow synaptic cleft. Inhibition of neurotransmitter reuptake with competitive inhibitors of transport, like AMPH, or nonexchanging transport inhibitors, like cocaine, results in DA accumulation in the synaptic cleft with increases in dopaminergic neurotransmission.

Neurotransmitter transporters engage in both homo- and heteroexchanges. Heteroexchange occurring between extracellular AMPH and its derivatives and the accumulated high intracellular concentrations of DA, 5-HT or NE was first described by Fischer and Cho (1979) in synaptosomes. The conventional model for neurotransmitter exchange is based on a mobile carrier-mediated sugar counterflow template seen in red cells.

Simulating Neurotransmitter Exchanges with the Conventional Alternating Model

The conventional SERT carrier model for net 5-HT accumulation (Fig. 4a, b) can easily be extended to simulate isotope exchange fluxes (Figs. 4i, k, m, 5h).

The conventional alternating carrier model of SERT (Adams and DeFelice 2003) predicts that at static head equilibrium the flux ratio of 5-HT should correspond to the relationship

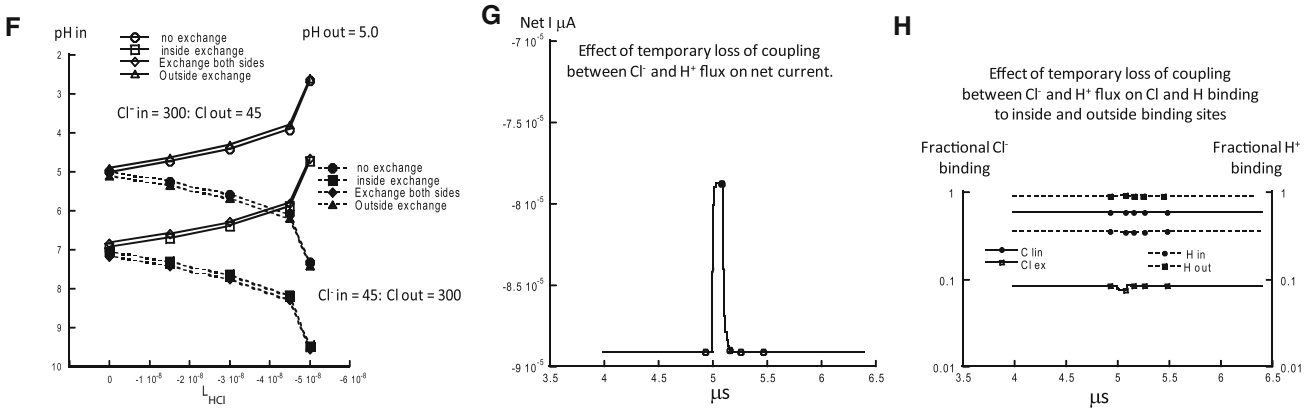

Fig. 6 continued

$$\frac{[5HT]_{in}}{[5HT]_{out}} = \left(\frac{[Na]_{out}}{[Na]_{in}}\right)^{n}$$

The conventional model predicts that replacing extracellular 140 mM Na^+ with 10 mM Na^+ should reduce inward 5-HT movement without substantially affecting 5-HT efflux. Also, at any fixed serotonin accumulation ratio and Na^+ ion distribution, the serotonin exchange flux ratio should be independent of external [5-HT]. None of these predictions accords with the experimental findings (Adams and DeFelice 2002, 2003).

An underreported prediction of the conventional alternating SERT carrier model is that there should be a biphasic relationship between steady-state 5-HT accumulation and membrane potential (Fig. 5e, f). Maximal 5-HT accumulation is predicted to reach an optimal value between 0 and –40 mV, depending on the net charge ascribed to the ligand carrier complex. The more negative the net charge, the higher the predicted accumulation of 5-HT and the more negative the membrane potential at the optimal accumulation. The reason for this biphasic accumulation is the reciprocal effect that the membrane potential has on inward and outward facing distributions of the electrically charged 5-HT–Na^2 carrier complex (Fig. 5f).

In contrast to the biphasic relationship of DA or 5-HT accumulation on membrane potential predicted by the conventional model of DAT, the frictional model predicts a continuous increase in DA or 5-HT accumulation as membrane potential is reduced from 50 to –150 mV (Fig. 5i). This accords with the experimental findings (Adams and DeFelice 2002, 2003).

Simulating AMPH/DA Exchange with the Frictional Model

The effects of altered extracellular Na^+ on unidirectional ligand fluxes via SERT expressed in human embryonic kidney cells differ from the predictions of the conventional alternating carrier model (Sitte et al. 2001). Reducing extracellular Na^+ from 140 to 10 mM increased efflux of labeled 1-methyl-4-phenylpyridinium (MPP) in exchange with *p*-chloroamphetamine (PCA) by threefold without significantly affecting influx. Thus, apparently, neurotransmitter exchange influx and efflux via SERT are independently modulated.

This finding is inconsistent with the alternating carrier model of exchange because any factor which affects efflux is predicted to affect influx proportionately to the same extent.

Although these experimental findings differ from the conventional model predictions, they are consistent with those of frictional model cotransport. This predicts that exchange influx is not affected by considerable reduction in external Na^+ concentration, whereas unidirectional efflux is enhanced by reduction of external Na^+ (Fig. 5k). The observed increase in DA efflux following reduction of extracellular Na^+ or Cl^- is explained by a reversal of the "sweeping away" effect of DA from the endofacial surface as convective drag by Na^+ influx is lessened by the reduced force exerted by the Na^+ gradient when external Na^+ is reduced from 140 to 10 mM.

Na^+ "Sensitivity" Anomalies of DA Efflux via DAT

Although multimodal changes in the operation of neurotransmitter transporters are inconsistent with the conventional model, there are several ways in which these transporters can be regulated. This makes interpretation of multimodal efflux difficult (Robertson et al. 2009).

The variable rates of AMPH-dependent DA efflux across DAT have been ascribed to an AMPH-dependent increase in intracellular Na^+, as monitored by intracellular Na^+ probes (Khoshbouei et al. 2003). This is qualitatively consistent with the conventional alternating model because increased intracellular Na^+ will enhance DA efflux. Similarly

AMPH-like drugs, e.g., PCA and methylene-dioxymethamphetamine (MDMA), induce an inward Na^+ current, whereas nonamphetamines, e.g., 5-HT, MPP^+ and tryamine, do not induce an inward Na^+ current and are less efficacious than AMOHs in inducing DA efflux (Hilber et al. 2005).

External Agents Which Modulate DA Transport via DAT: Protein Kinase C

Phosphorylation of DAT by protein kinase C (PKC) reduces both DA uptake via DAT and its surface expression (Reith et al. 1997). PKC activators—namely, phorbol esters—increase DA release (Kantor and Gnegy 1998), whereas PKC inhibition blocks the AMPH-mediated DA release from rat striatal slices, even after treatment with reserpine, which discharges DA from vesicles. Additionally, human DAT mutants that prevent DAT phosphorylation, or calmodulin kinase IIα (CAMKIIα) binding impair AMPH-dependent DA efflux (Fog et al. 2006).

Syntaxin 1A Interaction with DAT

Another way in which DA efflux can be altered by AMPH is via the protein receptor + 9r protein syntaxin 1A (SYN1A) interaction with the first 33 amino acids of the N-terminal chain of DAT. AMPH increases SYN1A binding to DAT. Cells overexpressing SYN1A have a greater AMPH-dependent DA efflux. In the absence of SYN1A, CAMKIIα does not activate DA efflux (Ciccone et al. 2008). SYN1A/CAMKIIα cells have increased sensitivity of DA efflux to membrane potential change. At –60 mV DA efflux is absent, but it is present in cells perfused with exogenous SYN1A (Binda et al. 2008).

Changes in Surface Expression of DAT Affect AMPH–DA Exchange Efflux

Until recently it was thought that AMPH enhances internalization of DAT (Saunders et al. 2000; Sulzer et al. 2005); however, in rat striatal synaptosomes, low AMPH (3 μM) concentrations cause a transient, cocaine-sensitive increase in surface expression of DAT, which remains higher than control for about 1 min (Johnson et al. 2005). This AMPH-dependent increase in DAT expression was blocked by tetanus or botulinum toxin C. These toxins cleave the *N*-ethyl-maleimide–sensitive factor (SNARE) in isolated neuroblastoma cells (Furman et al. 2009). These findings suggest that much of the initial AMPH-dependent stimulation of DA release could be ascribed to increased surface expression of DAT, rather than increased intrinsic efflux from the transporter.

Intrinsic Multimodal Transporter Activity Affecting DA Efflux

An unambiguous demonstration that there are at least two components to DA efflux via DAT has been obtained by monitoring the rates of DA release from outside–out membrane patches from transfected *Xenopus* oocytes expressing the transporter. DA efflux was measured simultaneously with voltage-clamp recording of the transmembrane currents and electrometric DA detection (Kahlig et al. 2005). A slow rate of DA release, consistent with AMPH/DA exchange, was detected at negative intracellular membrane potentials with low intracellular Na^+ (< 30 mM). A second, faster mode, more consistent with "channel-like" transport than a carrier process, was observed only above a membrane potential of +50 mV. Large numbers of DA molecules were released in millisecond bursts during "channel release," but this was blocked by external cocaine, stimulated by external AMPH and required intracellular Na^+. However, DA, when present on both sides of the membrane, inhibited this "channel" activity.

These bimodal DA-exchange conduction states observed with DAT in isolated membranes in conditions of voltage clamp and fixed ionic concentrations cannot be ascribed to changes in intracellular Na^+ or membrane potential as the membrane potential was voltage-clamped, so they are inconsistent with the predictions of the alternating transporter. However, they are easily reconcilable with the frictional model of DAT, as will be discussed.

Mutant hDATs with Enhanced Na^+ Sensitivity

A number of DAT mutants have differential DA influx and efflux sensitivities to altered intracellular Na^+ (Chen and Rudnick 2000). A mutant strain of human DAT, A599 V, has increased DA efflux over wild-type DAT at depolarizing potentials and increased sensitivity to intracellular Na^+ (Mazei-Robison et al. 2008). Both AMPH and methylphenidate inhibit DA release in the mutant DAT, A599 V, while they stimulate DA release from wild-type transporter. Another hDAT mutant, T62D, in contrast with A599 V, has reduced DA influx but, like A599 V, also has greatly increased AMPH-dependent DA efflux. This mutant transporter has enhanced sensitivity to membrane potential depolarization, activation occurring at around 0 mV instead of 50 mV, as observed in wild type (Guptaroy et al. 2009).

A New Interpretation of Multimodal DA Exchanges

The observations of intrinsic transporter activity in isolated membrane patches (Kahlig et al. 2005; Mazei-Robison

et al. 2008) imply that DAT has at least two intrinsic modes of exchange transport of DA. Multiple exchange modes are inconsistent with the conventional alternating transporter models. However, multiple rates of AMPH–DA exchange are consistent with a neurotransmitter transport model where the exchanging ligands are subject to variable frictional interactions with confluent ions in the constricted regions of the central pores of these transporters.

Small and transient decreases in the frictional interactions between Na^+ and neurotransmitter within the central pore will lead to transient increases in neurotransmitter release as the sweeping away effect is diminished. This permits cytosolic neurotransmitter to accumulate at the internal surface of the external exchange site, thus permitting higher rates of exchange. These effects are illustrated in Fig. 5 (a, b, l, m).

Enhanced slippage can be envisaged as being caused by small, transient increases in the width of the narrow part of the channel where close ligand encounters are enforced. This relaxation transiently reduces the frictional interactions which would normally sweep away the exchanging ligand entering the pore from the cytosol. Hence, a higher concentration of neurotransmitter from the cytosol accumulates at the endofacial surface of the neurotransmitter binding site, and this leads to a transient increase in exchange flux (Fig. 5b, m).

CLC Channel Structures in Relation to Cl^-/H^+ Exchange

The CLC family of Cl^- channels and transporters is present in all types of living organisms and shares a common 3D architecture (Dutzler 2007). The members of this family are located in either the plasma or the intracellular membranes; are involved in anion conductance, anion exchange and anion–proton exchange processes; and are important in organelle acidification and nitrate accumulation in plants.

The crystal structure of the prokaryotic *Escherichia coli* ecCLC Cl^-/H^+ transporter contains paired homodimer units (Dutzler 2007; Dutzler et al. 2003). Each subunit chain consists of duplicated halves. The C-terminal half contains six transmembrane helices, with an inverse sequence to the N-terminal half. This generates a 3D topology consisting of 12 antiparallel transmembrane domains. A narrow central channel, surrounded by structural components from each half, spans the length of the protein, joining two wider vestibules at the exo- and endofacial surfaces.

Mutation studies together with X-ray crystallographic studies have delineated four key amino acids important for proton coupling and Cl^- conductance within the ecCLC channels. An external Cl^- binding site was identified by X-ray crystallographic studies at E148 (Dutzler et al. 2003). Another Cl^- binding site is 1.5 nm distant from the external site, at E 203 at the opposite internal end of a narrow central chamber. A third Cl^- binding site is situated approximately midway between E148 and E203 in a narrow region, 0.46 nm wide, bounded on one side by the aromatic Y445 phenolate residue and on the other by the S107 hydroxyl residue (Fig. 6b).

The E148 carboxylate side chain is essential for coupled H^+ exchange with Cl^- (Accardi and Miller 2004). Mutation of E148 to glutamine, E148Q, or alanine, E148A, eliminates the increase in Cl^- conductance, seen at low pH. This is ascribed to the mobility of the carboxylate side chain, which in its anionic form occludes the external Cl^- binding site (Dutzler et al. 2003). High Cl^- in the external, or cytosolic, solution or protonation of the E148 carboxylate residue increases the likelihood of a high Cl^- conductance state by maintaining a "foot in the door" (Kuang et al. 2007) (Fig. 6a).

Glutamate at the equivalent position to 203 in CLC–ec is found in all CLC channels that act as Cl^-/H^+ exchangers, while valine at position 203 is found in pure Cl^- conductance channels (Accardi et al. 2005, 2006). E203 replacement with glutamine, E203Q, inhibits Cl^- conductance at neutral pH but not at pH 4.5 and abolishes Cl^-/H^+ exchange. However, the double mutant E148Q/E203Q fully restores Cl^- conductance. This finding suggests that the Cl^- and proton conductance pathways diverge at some point within the channel.

The Central Cl^- Binding Site

Replacing the centrally positioned tyrosine-445 phenolate residue with less bulky side chains, e.g., glycine, alanine or serine, alters the coupling Cl^-:H^+ ratios from 2:1 to around 8:1, as monitored by alterations in the nulling current of Cl^- dilution potentials and the extent of uphill H^+ movements across ecCLC channels incorporated into planar lipid membranes, whereas mutations of Y445 with phenylalanine or tryptophan retain similar Cl^-:H^+ coupling ratios to those found with tyrosine, i.e., 2 or 3:1 (Accardi et al. 2004; Walden et al. 2007). Thus, apparently, the width and perhaps the hydrophilicity of the narrow opening between Y445 and S107 determine the anion:proton coupling ratio and the specificity to Cl^- and bulkier anions, e.g., NO_3^- or SCN^-.

CLC Cl^-/NO_3^- Selectivity

Several plant isoforms of CLC channels function as $2NO_3^-$:$1H^+$ exchangers, instead of $2Cl^-/1\ H^+$ exchangers (De Angelo et al. 2006). The plant CLC transporter At-CLC, when expressed in *Xenopus* oocytes, mediates both NO_3^-/H^+ and Cl^-/H^+ exchange (Bergsdorf et al. 2009).

The key amino acids important for Cl^-, H^+ and NO_3^- flux selectivity and coupling have been identified. A single proline residue at the equivalent position to S168 in ecCLC at the central Cl^- binding site in CLC-5 favors NO_3^-/H^+, rather than Cl^-/H^+, exchanges (Bergsdorf et al. 2009). When expressed in *Xenopus* oocytes the mutated endosomal CLC-5 S168P results in NO_3^-/H^+, instead of Cl^-/H^+, exchange (Zifarelli and Pusch 2009). In ecCLC the equivalent S168 to CLC-5 is S107 on the opposing side of the central exchange channel from Y445 (Accardi and Miller 2004). Anion substitution studies show that the tight Cl^-/H^+ coupling ratios are no longer preserved when larger anions, e.g., SCN^- and NO_3^-, are substituted for Cl^- (Accardi et al. 2005; Bergsdorf et al. 2009).

As with eCl^-CLC, the mutation E203A abolished coupling between H^+ and Cl^- currents and the mutation E270A abolished the currents altogether (Accardi et al. 2004, 2005). The At-CLC channel resembles ec-CLC in that the uncoupled anion conductances of both Cl^- and NO_3^- could be restored by the double mutation E270A/E203A (Bergsdorf et al. 2009).

These experiments indicate that the exchange pathways for Cl^- or NO_3^- and H^+ are divergent at some point within the body of the transporter. This finding is inconsistent with the conventional model of the alternating transporter that requires the canonical pathways for exchange flux to follow a strict cyclic configuration.

Stoichiometry of Cl^-/H^+ Exchange

The Cl^-/H^+ coupling mode of CLC operation was first detected as a deviation from the expected reversal potential in voltage-clamped *I–V* curves, when purified eCl^-CLC transporters incorporated into lipid membranes were exposed to a 300:45 mM 6.7-fold Cl^- gradient with uniformly distributed pH. Similar deviations in the *I–V* curves were obtained with pH gradients and a uniform Cl^- distribution. Uphill Cl^- movement into liposomes was detected using a Cl^--sensitive dye incorporated within the liposomes. Uphill proton inflow into the liposomes in response to an outward Cl^- gradient was detected by monitoring the pH increase of the external solution with a glass pH electrode (Accardi and Miller 2004).

Accurate determination of proton flux remains a problem in assessing Cl^-/H^+ kinetics. Proton influx has been measured by intracellular ΔpH monitored with a ratiometric fluorescence dye (Alekov and Fahlke 2009). However, monitoring true rates of proton influx by intracellular pH change is complicated because estimates of intracellular buffering capacity (β) are imprecise and overestimation of effective cell volume leads to overestimation of Cl^-/H^+ exchange ratios.

Additionally, measurements of proton efflux from liposomes containing high concentrations of the purified CLC-ec1 transporter by extracellular pH recording may be obscured by proton accumulation within unstirred layers adjacent to the membrane with consequent proton backflux and underestimation of flux.

Ion fluxes measured across transfected mammalian cell-attached patches expressing CLC-4 channels and using nonstationary noise analysis demonstrate an absence of saturation of Cl^- flux, even at very high positive voltages, together with high unitary transport rates (Alekov and Fahlke 2009). These experiments suggest that CLC-4 has two operational modes, Cl^- binding resulting in transition from slippage to exchanger mode.

Nevertheless, in the uncoupled "slippage" mode, Cl^--selective CLC pores have a high Cl^- conductance (5×10^5 ions s^{-1}) (Accardi et al. 2004; Accardi and Miller 2004; Alekov and Fahlke 2009). These very high Cl^- conductance rates are consistent with ion flux via an open channel. Although Cl^-/H^+ antiport is 10 times slower than in the slippage mode, it is still 10-fold faster than any other reported exchange mode (Alekov and Fahlke 2009; Brahm 1977; Brahm and Wieth 1977; Hille 2001).

Until recently, it had been accepted that the exchange mode of the Cl^-/H^+ exchanger was explicable by a single alternating site with a fixed $2Cl^-$:$1H^+$ stoichiometry antiporter. However, this view has been undermined by some key observations. The claim that there is fixed stoichiometry of Cl^-/H^+ flux has been refuted. Substitution of bulkier anions, e.g., NO_3^- or SCN^- for Cl^-, partially uncouples proton flux with anion flux so that anion:proton flux ratios greatly exceeding 2 anions:1 proton are observed (Accardi et al. 2005, 2006; Alekov and Fahlke 2009; Bergsdorf et al. 2009; Lim and Miller 2009). The fast rate of Cl^- flux in both "slippage" and exchange modes and the lack of apparent saturation of unit conductance with voltage indicate that there is no large conformational change involved in either transport mode (Alekov and Fahlke 2009). This view is supported by cross-linkage experiments within CLC-ecl constructs in which as many as four cross-links aimed at constraining large conformational change did not alter Cl^- conductance or Cl^-/H^+ exchange (Nguitragool and Miller 2007). These data provide a correlation of cotransport function with CLC channel/transporter protein structure that is currently more precise than with any other transporter.

Discordant Features of CLC Transporters with Conventional Alternating Transporters

Several features of CLC channels/carriers do not accord well with the perceived view of a conventional single alternating site model of Cl^-/H^+ antiporter.

- There are three Cl^- binding sites (Dutzler et al. 2003) distributed at intervals of 0.7 nm across the central channel; the routes for Cl^- and H^+ are not entirely congruent (Accardi et al. 2005).
- The lack of saturability of Cl^- flux at high positive membrane potential is inconsistent with any large-scale protein conformational changes (Alekov and Fahlke 2009).
- Multiple intraprotein cross-linkages in which protein movements are constrained yet the transport properties of CLC are preserved are also inconsistent with any large-scale conformational changes (Nguitragool and Miller 2007).
- The stoichiometry between Cl^- and H^+ antiport is variable. This variability is even more obvious between NO_3^- or SCN^- and H^+ than with Cl^- (Bergsdorf et al. 2009; Walden et al. 2007).
- Additionally, there are multiple conductance states reported for both exchange and slippage modes (Alekov and Fahlke 2009).

A Frictional Model for Cl^-/H^+ Exchange Flux via CLC Transporters

The general frictional cotransport model developed here to explain sodium-dependent glucose transport and neurotransmitter symport and exchange can be adapted to a model that explains the apparently anomalous features of Cl^-/H^+ exchange so far encountered (Fig. 6c, d).

The frictional coupled model, as outlined in Fig. 6b, readily simulates the deviations from ideality of the current–voltage relationships, observed initially by Accardi et al. (2004) and Accardi and Miller (2004). The model is consistent with the variable Cl^-/H^+ stoichiometry (Alekov and Fahlke 2009; Lim and Miller 2009; Miller and Nguitragool 2009; Walden et al. 2007). It readily accommodates the 1.5 nm distance between the separate exchange sites for Cl^-/H^+ at the external and internal glutamate at E148 and E203. The sites available for Cl^-/H^+ exchange at either end of the narrow central channel rationalize uphill proton movement generated by a Cl^- gradient by the same mechanism as proposed already for glucose exchange and transport via GLUT1 (Naftalin 2008a).

However, these exchange sites do not account for the selectivity and cotransport roles of S107/Y445 at the central position within the channel. Frictional interactions of anions with the serine or proline OH^- side chains at position 107 in this narrow central region are likely determinants of Cl^- or NO_3^- selectivity. It seems more probable that these occur between Cl^- and OH^- anions rather than with hydrated H^+ ions as the collisional interactions are most likely to be propulsive. Cl^-/OH^- symport is kinetically exactly equivalent to Cl^-/H^+ antiport. An inwardly directed Cl^- concentration gradient will thus lead to proton accumulation adjacent to the external Cl^- binding site at E148 as OH^- is depleted from this region. Proton accumulation will enhance Cl^-/H^+ exchange at the external site (Fig. 6b).

The simulations shown in Fig. 6e, f indicate that Cl^-:H^+ exchange at the external site and a Cl^-:OH^- symporter within the central part of the channel give the optimal uphill Cl^- and proton accumulations. A second exchange at the inner-site Cl binding is unnecessary and in some cases counterproductive.

Bimodal Cl^-/H^+ Exchange States

Multiple modes of net Cl^- and Cl^-/H^+ exchange flux have been observed in CLC transporters (Alekov and Fahlke 2009), similar to those observed with DA-exchange transport in DAT (Kahlig et al. 2005). The frictional cotransport model outlined, as well as simulating Cl^-/H^+ or AMPH/DA exchanges, can be readily adapted to explain the high- and low-conductance states of Cl^- conductance and Cl^-/H^+ exchange flux.

Substitution of tyrosine residues at position 445 by smaller alanine or glycine side chain residues increases Cl^- slippage in inverse proportion to the side chain mass and indicates that the width of the channel between the side chains at positions 445 and 107 on the opposite channel surface, normally 0.45 nm, affects the coupling ratio (Walden et al. 2007) (Fig. 6b). This constriction could force OH^- and Cl^- into close proximity as they traverse the channel and thereby raise the probability of frictional collisions, thus increasing the coupling coefficient, $L_{H\text{-}Cl}$. Conversely, widening the gap by 0.3–0.5 nm reduces the coupling coefficient to practically zero (Walden et al. 2007) (Fig. 6b). Thus, any transient channel widening, perhaps as a result of proton accumulation within the channel, will reduce frictional coupling between Cl^- flux and OH^- flux in the central zone and thereby increase ion "slippage." Thus, transient alterations in the channel width could lead to reversible changes in the frictional coefficients and thereby generate multiple conductance states.

This multimodal behavior is readily simulated with the model by reversible switching on or off of the cotransport coefficient $L_{H\text{-}Cl}$ (Fig. 6g, h). Specifically, in the presence of an inwardly directed pH gradient, reduction in the coupling coefficient will increase the local Cl^- concentration at the endofacial surface of the external exchange site and thereby increase the rate of H^+/Cl^- (Fig. 6h).

Structural Implications of the Alternating Transport Model: Evidence of Conformation Change Leading to Site Occlusion

The determinate asymmetric alternating carrier heuristic has had an overwhelming influence on perceptions of transporter structures. The model implies that a single centrally placed binding site exists within the membrane transporter whose exposure "alternates" either when complexed to ligand(s) or when vacant. The thermodynamic forces causing ligand flux and flux coupling are transmitted by gradients of the mobile ligand carrier complex rather than the electrochemical potentials of the ligands themselves. Thus, ligand-induced changes in protein conformation are considered to generate the forces that alter the affinity, assemble the ligand complex and mobilize the ligand binding site within the transporter. The number of ligand binding sites is expected to correlate with the "stoichiometry" of transport.

There is much current debate regarding the structural criteria that characterize carrier and channel transport. What were once considered to be distinguishing features of channels or transporters are now recognized as being shared between channels, facilitative transporters and cotransporters. Diallinas (2008) has succinctly suggested that channels have a continuous gated pore, whereas transporters have an interrupted pore. Although several crystal structures of bacterial transporter proteins have been described in support of this view, there are also several exceptions. In particular, a recent crystal structure of the urea transporter from the bacterium *Desulfovibrio vulgaris* showed a core containing a membrane-spanning pore with a selectivity filter which can accommodate several dehydrated urea molecules. This urea transporter operates as a channel, although urea transport is inhibited by phloretin and shows saturation kinetics (K_d) 2.3 ± 0.14 mM (Levin et al. 2009). The crystal structure suggests that several dehydrated urea molecules can simultaneously move through the transporter, spanning the channel by stepwise H-bond interactions with a ladder of conveniently placed oxygen atoms present in side chains and a transmembrane helical backbone. No constriction is present in this channel, yet except for its exceptionally high turnover rate, it operates like a transporter rather than a channel.

A key component of the alternating carrier model is that the central binding site should have both inward- and outward-facing conformations. Transporter conformations have been described where a vestibular opening of the central channel faces either inward, as with *E. coli* LacY (Abramson et al. 2004a; Abramson et al. 2004b; Abramson et al. 2003; Guan and Kaback 2006), or outward, as with LeuT and MPH1. An outward-facing conformation in LeuT, where both the inside and outside sites are occluded from the bathing solutions, can be modified to an open state by low-affinity binding of Trp to arginine and aspartate residues at the extracellular vestibule exit. Two other lower-affinity Trp binding sites have recently been uncovered in the outward-facing vestibule (Singh et al. 2008; Singh et al. 2007). It is proposed that ligand binding to the low-affinity binding sites triggers the conformational changes leading to ligand access to the central high-affinity site.

Other support for the view that the transporter protein first binds to its substrate, then encloses and occludes the substrate from both external and internal solutions, comes from two complementary studies. The *Vibrio parahaemolyticus* sodium/galactose symporter (vSGLT) has 14 transmembrane helices, crystallized in an inward facing conformation which occludes galactose from the internal solution (Faham et al. 2008). The prokaryotic nucleobase cation symport 1 (NSC1) transporter from *Microbacterium liquefaciens* crystallizes in the outwardly facing apocrystal structure binds; encloses its substrate, benzyl-hydantoin; and occludes it from both external and internal solutions (Weyand et al. 2008). A dynamic simulation of the conformational changes during inversion of the central binding sites required to generate ligand translocation has been obtained by combined inside- and outside-facing conformations of these proteins (Faham et al. 2008).

However, crystallographic images of several transport proteins show that unilateral occlusion occurs independently of any opening event on the alternate side (Faham et al. 2008). Thus, occlusion with ligand at the central site does not automatically or instantaneously lead to contralateral opening, as the alternating model would imply.

Dynamic studies of the conformational changes in LacY lactose-proton symporter monitored with double electron resonance studies between paired nitroxide-labeled double cysteine mutants have measured the changes in interhelical separation at the cytoplasmic and external surfaces of the central cavity. Specifically, transported galactoside binding reduced the interhelical distance at the cytoplasmic side by ≈1.6 nm, whereas on the external side there was an increase of ≈1 nm, indicating reciprocal cleft opening at the external surface and closure at the inside (Majumdar et al. 2007; Smirnova et al. 2007).

It is implied that ligand binding can generate conformational changes leading to ligand occlusion from the ipsilateral bathing solutions. Although these conformational changes are associated with contralateral conformational changes, they are viewed separately and have not yet been subjected to time-correlation studies. Thus, at present it is unclear if there is a pivotal lever-arm linkage between the inward and outward conformations, as is implied by the sequential diagrams (Faham et al. 2008).

Is the Slow Rate of Carrier Transport Related to Conformational Change?

Until recently it was considered that the "turnover number" of the carrier transport process is several orders slower than most channel-mediated transport processes. However, since ligand association and dissociation events with the external binding sites of DAT have a high frequency but transport events occur infrequently, it is evident that the "slowness" of this "carrier-mediated transport system" is due to the paucity of transport events, rather than to their sluggish rates of translation (Schwartz et al. 2003, 2005). Additionally, in CLC transporters, the rate of Cl^-:H^+ exchange is much faster (10^5 s^{-1}) than is consistent with the large conformational changes that have been considered necessary to accommodate these changes (Alekov and Fahlke 2009) and the urea diffusion rates through mammalian and bacterial transporters occur at similar rates, 10^4–10^6 s^{-1} (MacIver et al. 2008).

Is Channel Occlusion Necessary to Create and Sustain a Ligand Gradient?

Occlusion of the transporter pathway is considered necessary to prevent both leakage of unwanted ligands via the open pathway and maintenance to solute gradients. However, the convective diffusion process illustrated in Figs. 4c and 5a generates and maintains stationary-state solute accumulations without an occlusive barrier (Eq. 47; Figs. 4j, 5g, i, j).

As GLUTs and SGLT permit osmotic pressure–induced water flow and SGLT permits electrical current conductance and Na^+ conductance (Naftalin 2008b; Zeuthen and Zeuthen 2007; Zeuthen et al. 2007), it follows that they possess some channel properties permitting uninterrupted hydraulic pressure or electrical potential transmission across the length of the transporter.

As Na^+, hydroxonium or hydroxyl ions are so small, it is arguable that they might pass below the size discriminator set for all other ligands within transporters. However, both osmotic water permeability in GLUTs 1 and 2 (Zeuthen and Zeuthen 2007; Zeuthen et al. 2007) and Na^+ currents in SGLT (Mackenzie et al. 1996, 1998) are affected by glucose, so these leaks cannot be entirely independent of the other ligand flows. Thus, attributing the simple "basal rates" to leak or unstimulated rates of ligand flow is probably an oversimplified view.

Accelerated Exchange

Accelerated exchange is another criterion of a mobile carrier (Fischer and Cho 1979; Wilbrandt and Rosenberg 1961). Since accelerated exchange also occurs at "simple" inorganic binding sites (Saint-Martin et al. 1988), this can no longer be considered a unique signifier of biological carriers.

Despite having no capacity for accelerated exchange, several transporters, including GLUT 4 (Dauterive et al. 1996), are nonetheless regarded as carriers because they selectively facilitate glucose transport with high affinity and can be inhibited by standard competitive and non-competitive inhibitors.

The high activation energy, or Q10, of the glucose transporter in comparison with most diffusion processes via channels (Brahm 1983; Naftalin and Arain 1999) is shared by any catalytic process having a high activation energy (Li, Petroski and El-Sayed 2000), so it does not necessarily signify a mediated carrier transport.

Thus, transporters mediating exchange and uphill cotransport can be considered as partially occluded channels which lie within a spectrum of transmembrane structures from totally occluding channels, as seen with Na^+,K^+-ATPase, which requires a large chemical stimulus to generate an opening or transport event (Morth et al. 2009), to semiocclusive channels like GLUTs, SGLT, DAT and SERT to minimally occlusive channels such as ligand-gated channels and voltage-gated CLC channels to fully open channels as exemplified by urea channels (MacIver et al. 2008) where ligand flow is unhindered at all times.

The Structural Requirements of the Fixed Multisite Model and the Frictional Cotransport Model

The criteria for fixed-site exchange transporters or friction-driven cotransporters are easily accommodated with known transporter structures. All that is required is a stricture within the transport pathway where all the cotransported ligands can converge and interact frictionally *en passant*. The pathways for cotransporter ligands need not be entirely congruent, as has been observed with H^+:Cl^- exchange (Accardi et al. 2005). It is also possible that parallel pathway options with different ligand selectivities provide an explanation for selectivity mutants (Naftalin et al. 2007; Van Camp et al. 2007). Additionally, as the "gearing" of cotransported ligand flux ratios depends not on a fixed stoichiometric ratio but on the ratio of coupling coefficients with the straight permeability coefficients (Eq. 47), there is no requirement for binding sites to accommodate the exact number of driving ligands, e.g., $2Na^+$ to generate the observed stoichiometry with SGLT or DAT. Multiple binding sites within the transport protein extending across the entire length of the transport route have also been observed for Trp binding in LeuT (Singh et al. 2008) and in CLC (Dutzler 2007; Dutzler et al. 2003). Multiple sites permit geminate recombination of ligands, which slows the

transport rates across the ensemble of sites (Leitch and Carruthers 2009).

Possibly too narrow a view of the channel "interruption" has been assigned to bistable gates within transporters and channels (Jardetzky 1966). A channel stricture may have other important roles, as a condenser of ligand flows enforcing frictional interactions within the confined space available or as a barrier, in advance of which entrained ligands in downstream flows accumulate and behind which ligands become depleted and thus act as a rectifier and capacitor (Kedem and Katchalsky 1963a, 1963b, 1963c; Patlak et al. 1963). Additionally, a partial occlusion can act as a semipermeable barrier permitting osmotic gradients and flows to be generated by the transported ligands (Naftalin 2008b).

Acknowledgements I wish to acknowledge the generous help and useful discussions I have had during preparation of this review with Professor Louis J DeFelice, Departments of Physiology and Biophysics Virginia Commonwealth University (Richmond, VA) and Professor Anthony Carruthers Departments of Biochemistry and Molecular Pharmacology University of Massachussetts Medical School.

References

Abramson J, Smirnova I, Kasho V, Verner G, Kaback HR, Iwata S (2003) Structure and mechanism of the lactose permease of *Escherichia coli*. Science 301:610–615

Abramson J, Iwata S, Kaback HR (2004a) Lactose permease as a paradigm for membrane transport proteins [review]. Mol Membr Biol 21:227–236

Abramson J, Kaback HR, Iwata S (2004b) Structural comparison of lactose permease and the glycerol-3-phosphate antiporter: members of the major facilitator superfamily. Curr Opin Struct Biol 14:413–419

Accardi A, Miller C (2004) Secondary active transport mediated by a prokaryotic homologue of ClC Cl^- channels. Nature 427:803–807

Accardi A, Kolmakova-Partensky L, Williams C, Miller C (2004) Ionic currents mediated by a prokaryotic homologue of CLC Cl^- channels. J Gen Physiol 123:109–119

Accardi A, Walden M, Nguitragool W, Jayaram H, Williams C, Miller C (2005) Separate ion pathways in a Cl^-/H^+ exchanger. J Gen Physiol 126:563–570

Accardi A, Lobet S, Williams C, Miller C, Dutzler R (2006) Synergism between halide binding and proton transport in a CLC-type exchanger. J Mol Biol 362:691–699

Adams SV, DeFelice LJ (2002) Flux coupling in the human serotonin transporter. Biophys J 83:3268–3282

Adams SV, DeFelice LJ (2003) Ionic currents in the human serotonin transporter reveal inconsistencies in the alternating access hypothesis. Biophys J 85:1548–1559

Alekov AK, Fahlke C (2009) Channel-like slippage modes in the human anion/proton exchanger ClC-4. J Gen Physiol 133:485–496

Baker GF, Naftalin RJ (1979) Evidence of multiple operational affinities for D-glucose inside the human erythrocyte membrane. Biochim Biophys Acta 550:474–484

Baker GF, Widdas WF (1973) Asymmetry of facilitated transfer system for hexoses in human red-cells and simple kinetics of a 2 component model. J Physiol 231:143–165

Bergsdorf EY, Zdebik AA, Jentsch TJ (2009) Residues important for nitrate/proton coupling in plant and mammalian CLC transporters. J Biol Chem 284:11184–11193

Binda F, Dipace C, Bowton E, Robertson SD, Lute BJ, Fog JU, Zhang M, Sen N, Colbran RJ, Gnegy ME, Gether U, Javitch JA, Erreger K, Galli A (2008) Syntaxin 1A interaction with the dopamine transporter promotes amphetamine-induced dopamine efflux. Mol Pharmacol 74:1101–1108

Brahm J (1977) Temperature-dependent changes of chloride transport kinetics in human red cells. J Gen Physiol 70:283–306

Brahm J (1983) Kinetics of glucose transport in human erythrocytes. J Physiol 339:339–354

Brahm J, Wieth JO (1977) Separative pathways for urea and water, and for chloride in chicken erythrocytes. J Physiol 266:727–749

Carruthers A, Dezutter J, Ganguly A, Devaskar S (2009) Will the original glucose transporter isoform please stand up! Am J Physiol Endocrinol Metab 297:E836–E848

Centelles JJ, Kinne RK, Heinz E (1991) Energetic coupling of Na–glucose cotransport. Biochim Biophys Acta 1065:239–249

Chen JG, Rudnick G (2000) Permeation and gating residues in serotonin transporter 1. Proc Natl Acad Sci USA 97:1044–1049

Chen XZ, Coady MJ, Jackson F, Berteloot A, Lapointe JY (1995) Thermodynamic determination of the Na^+: glucose coupling ratio for the human SGLT1 cotransporter. Biophys J 69:2405–2414

Chen XZ, Coady MJ, Jalal F, Wallendorff B, Lapointe JY (1997) Sodium leak pathway and substrate binding order in the Na^+–glucose cotransporter. Biophys J 73:2503–2510

Ciccone MA, Timmons M, Phillips A, Quick MW (2008) Calcium/calmodulin-dependent kinase II regulates the interaction between the serotonin transporter and syntaxin 1A. Neuropharmacology 55:763–770

Cloherty EK, Heard KS, Carruthers A (1996) Human erythrocyte sugar transport is incompatible with available carrier models. Biochemistry 35:10411–10421

Dauterive R, Laroux S, Bunn R, Chaisson A, Sanson T, Reed B (1996) C-terminal mutations that alter the turnover number for 3-*O*-methylglucose transport by GLUT1 and GLUT4. J Biol Chem 271:11414–11421

De Angelo A, Monachello D, Ephritikhine G, Frachisse JM, Thomine S, Gambale F, Barbier-Brygoo H (2006) The nitrate/proton antiporter AtCLCa mediates nitrate accumulation in plant vacuoles. Nature 442:939–942

Deves R, Krupka RM (1981) Evidence for a two-state mobile carrier mechanism in erythrocyte choline transport: effects of substrate analogs on inactivation of the carrier by *N*-ethylmaleimide. J Membr Biol 61:21–30

Diallinas G (2008) Biochemistry. An almost-complete movie. Science 322:1644–1645

DiPolo R, Beauge L (2006) Sodium/calcium exchanger: influence of metabolic regulation on ion carrier interactions. Physiol Rev 86:155–203

Dutzler R (2007) A structural perspective on ClC channel and transporter function. FEBS Lett 581:2839–2844

Dutzler R, Campbell EB, MacKinnon R (2003) Gating the selectivity filter in ClC chloride channels. Science 300:108–112

Eddy A (1982) Mechanisms of solute transport in selected eukaryotic micro-organisms. Adv Microb Physiol 23(1–78):269–270

Edwards PA (1973) Evidence for the carrier model of transport from the inhibition by *N*-ethylmaleimide of choline transport across the human red cell membrane 2. Biochim Biophys Acta 311:123–140

Ege R (1927) The dispersed phase of the blood corpuscles 1. Biochem J 21:967–970

Ellory JC, Guizouarn H, Borgese F, Bruce LJ, Wilkins RJ, Stewart GW (2009) Review. Leaky Cl^-HCO_3-exchangers: cation fluxes

via modified AE1. Philos Trans R Soc Lond B Biol Sc. 364:189–194

Eraly SA (2008) Implications of the alternating access model for organic anion transporter kinetics. J Membr Biol 226:35–42

Erreger K, Grewer C, Javitch JA, Galli A (2008) Currents in response to rapid concentration jumps of amphetamine uncover novel aspects of human dopamine transporter function. J Neurosci 28:976–989

Eskandari S, Wright EM, Loo DD (2005) Kinetics of the reverse mode of the Na^+/glucose cotransporter. J Membr Biol 204:23–32

Essig A, Caplan SR (1989) Water movement: does thermodynamic interpretation distort reality? Am J Physiol 256:C694–C698

Faham S, Watanabe A, Besserer GM, Cascio D, Specht A, Hirayama BA, Wright EM, Abramson J (2008) The crystal structure of a sodium galactose transporter reveals mechanistic insights into Na^+/sugar symport. Science 321:810–814

Finkelstein A (1987) Water movement through lipid bilayers, pores, and plasma membranes: theory and reality. Wiley, New York

Fischer JF, Cho AK (1979) Chemical release of dopamine from striatal homogenates: evidence for an exchange diffusion model 1. J Pharmacol Exp Ther 208:203–209

Fog JU, Khoshbouei H, Holy M, Owens WA, Vaegter CB, Sen N, Nikandrova Y, Bowton E, McMahon DG, Colbran RJ, Daws LC, Sitte HH, Javitch JA, Galli A, Gether U (2006) Calmodulin kinase II interacts with the dopamine transporter C terminus to regulate amphetamine-induced reverse transport. Neuron 51:417–429

Furman CA, Chen R, Guptaroy B, Zhang M, Holz RW, Gnegy M (2009) Dopamine and amphetamine rapidly increase dopamine transporter trafficking to the surface: live-cell imaging using total internal reflection fluorescence microscopy. J Neurosci 29:3328–3336

Geck P (1971) Properties of a carrier model for transport of sugars by human erythrocytes. Biochim Biophys Acta 241:462–472

Ginsburg H, Stein WD (1975) Zero-*trans* and infinite-*cis* uptake of galactose in human erythrocytes. Biochim Biophys Acta 382:353–368

Ginzburg BZ, Katchalsky A (1963) The frictional coefficients of the flows of non-electrolytes through artificial membranes. J Gen Physiol 47:403–418

Guan L, Kaback HR (2006) Lessons from lactose permease. Annu Rev Biophys Biomol Struct 35:67–91

Guptaroy B, Zhang M, Bowton E, Binda F, Shi L, Weinstein H, Galli A, Javitch JA, Neubig RR, Gnegy ME (2009) A juxtamembrane mutation in the N terminus of the dopamine transporter induces preference for an inward-facing conformation. Mol Pharmacol 75:514–524

Hankin BL, Stein WD, Lieb WR (1972) Rejection criteria for asymmetric carrier and their application to glucose transport in human red blood-cell. Biochim Biophys Acta 288:114–126

Hilber B, Scholze P, Dorostkar MM, Sandtner W, Holy M, Boehm S, Singer EA, Sitte HH (2005) Serotonin-transporter mediated efflux: a pharmacological analysis of amphetamines and non-amphetamines. Neuropharmacology 49:811–819

Hilgemann DW, Lu CC (1999) GAT1 (GABA:Na^+:Cl^-) cotransport function. Database reconstruction with an alternating access model. J Gen Physiol 114:459–475

Hille B (2001) Ion channels of excitable membranes. Sinauer, Sunderland, MA

Holman GD, Naftalin RJ (1975) Galactose transport across the serosal border of rabbit ileum and its role in intracellular accumulation 9. Biochim Biophys Acta 382:230–245

Holman GD, Naftalin RJ (1976) Transport of 3-*O*-methyl D-glucose and beta-methyl D-glucoside by rabbit ileum. Biochim Biophys Acta 433:597–614

Jardetzky O (1966) Simple allosteric model for membrane pumps. Nature 211:969–970

Jarvis SM, Hammond JR, Paterson AR, Clanachan AS (1983) Nucleoside transport in human erythrocytes. A simple carrier with directional symmetry in fresh cells, but with directional asymmetry in cells from outdated blood. Biochem J 210:457–461

Johnson LA, Furman CA, Zhang M, Guptaroy B, Gnegy ME (2005) Rapid delivery of the dopamine transporter to the plasmalemmal membrane upon amphetamine stimulation. Neuropharmacology 49:750–758

Joost HG, Bell GI, Best JD, Birnbaum MJ, Charron MJ, Chen YT, Doege H, James DE, Lodish HF, Moley KH, Moley JF, Mueckler M, Rogers S, Schürmann A, Seino S, Thorens B (2002) Nomenclature of the GLUT/SLC2A family of sugar/polyol transport facilitators. Am J Physiol Endocrinol Metab 282:E974–E976

Kahlig KM, Binda F, Khoshbouei H, Blakely RD, McMahon DG, Javitch JA, Galli A (2005) Amphetamine induces dopamine efflux through a dopamine transporter channel. Proc Natl Acad Sci USA 102:3495–3500

Kanner BI (1978) Active transport of gamma-aminobutyric acid by membrane vesicles isolated from rat brain. Biochemistry 17:1207–1211

Kantor L, Gnegy ME (1998) Protein kinase C inhibitors block amphetamine-mediated dopamine release in rat striatal slices. J Pharmacol Exp Ther 284:592–598

Kedem O, Caplan SR (1965) Degree of coupling and its relation to efficiency of energy conversion. Trans Faraday Soc 61:1897–1911

Kedem O, Katchalsky A (1963a) Permeability of composite membranes. 1. Electric current, volume flow and flow of solute through membranes. Trans Faraday Soc 59:1918–1930

Kedem O, Katchalsky A (1963b) Permeability of composite membranes. 2. Parallel elements. Trans Faraday Soc 59:1931–1940

Kedem O, Katchalsky A (1963c) Permeability of composite membranes. 3. Series array of elements. Trans Faraday Soc 59:1941–1953

Kessler M, Semenza G (1983) The small-intestinal Na^+, D-glucose cotransporter: an asymmetric gated channel (or pore) responsive to delta psi. J Membr Biol 76:27–56

Khoshbouei H, Wang H, Lechleiter JD, Javitch JA, Galli A (2003) Amphetamine-induced dopamine efflux. A voltage-sensitive and intracellular Na^+-dependent mechanism. J Biol Chem 278:12070–12077

Klein MJ (1955) Principle of detailed balance. Phys Rev 97:1446–1447

Kondepudi DK, Prigogine I (1998) Modern thermodynamics: from heat engines to dissipative structures. Wiley, Chichester, UK

Krupka RM (1990) Expression of substrate specificity in facilitated transport systems. J Membr Biol 117:69–78

Kuang Z, Mahankali U, Beck TL (2007) Proton pathways and H^+/Cl^-stoichiometry in bacterial chloride transporters. Proteins 68:26–33

Lapointe J, Sasseville L, Longpré J (2009) Alternating carrier models and the energy conservation laws. Biophys J 97:2648–2650

LeFevre PG, LeFevre ME (1952) The mechanism of glucose transfer into and out of the human red cell. J Gen Physiol 35:891–906

Leitch JM, Carruthers A (2009) Alpha- and beta-monosaccharide transport in human erythrocytes. Am J Physiol 296:C151–C161

Levin E, Quick M, Zhou M (2009) Crystal structure of a bacterial homologue of the kidney urea transporter. Nature 462:757–761

Levy L, Warr O, Attwell D (1998) Stoichiometry of the glial glutamate transporter GLT-1 expressed inducibly in a Chinese hamster ovary cell line selected for low endogenous Na^+-dependent glutamate uptake. J Neurosci 18:9620–9628

Lewis GN (1925) A new principle of equilibrium. Proc Natl Acad Sci USA 11:179–183

Li Y, Petroski J, El-Sayed M (2000) Activation energy of the reaction between hexacyanoferrate(III) and thiosulfate ions catalyzed by platinum nanoparticles. J Phys Chem B Condens Matter Mater Surf Interfaces Biophys 104:10956–10959

Lieb WR, Stein WD (1974) Testing and characterizing the simple carrier. Biochim Biophys Acta 373:178–196

Lim HH, Miller C (2009) Intracellular proton-transfer mutants in a CLC Cl^-/H^+ exchanger. J Gen Physiol 133:131–138

Lowe AG, Walmsley AR (1986) The kinetics of glucose transport in human red blood cells. Biochim Biophys Acta 857:146–154

MacIver B, Smith C, Hill W, Zeidel M (2008) Functional characterization of mouse urea transporters UT-A2 and UT-A3 expressed in purified *Xenopus laevis* oocyte plasma membranes. Am J Physiol 294:F956–F964

Mackenzie B, Loo DD, Panayotova-Heiermann M, Wright EM (1996) Biophysical characteristics of the pig kidney Na^+/glucose cotransporter SGLT2 reveal a common mechanism for SGLT1 and SGLT2. J Biol Chem 271:32678–32683

Mackenzie B, Loo DD, Wright EM (1998) Relationships between Na^+/glucose cotransporter (SGLT1) currents and fluxes. J Membr Biol 162:101–106

Majumdar DS, Smirnova I, Kasho V, Nir E, Kong X, Weiss S, Kaback HR (2007) Single-molecule FRET reveals sugar-induced conformational dynamics in Lac. Proc Natl Acad Sci USA 104:12640–12645

Mazei-Robison MS, Bowton E, Holy M, Schmudermaier M, Freissmuth M, Sitte HH, Galli A, Blakely RD (2008) Anomalous dopamine release associated with a human dopamine transporter coding variant. J Neurosci 28:7040–7046

Mikulecky DC (2001) Network thermodynamics and complexity: a transition to relational systems theory. Comput Chem 25:369–391

Miller DM (1971) The kinetics of selective biological transport. V. Further data on the erythrocyte–monosaccharide transport system. Biophys J 11:915–923

Miller C, Nguitragool W (2009) A provisional transport mechanism for a chloride channel-type Cl^-/H^+ exchanger. Philos Trans R Soc B-Biol Sci 364:175–180

Morth J, Poulsen H, Toustrup-Jensen M, Schack V, Egebjerg J, Andersen J, Vilsen B, Nissen P (2009) The structure of the Na^+, K^+-ATPase and mapping of isoform differences and disease-related mutations. Philos Trans R Soc B-Biol Sci 364:217–227

Naftalin RJ (2008a) Alternating carrier models of asymmetric glucose transport violate the energy conservation laws. Biophys J 95:4300–4314

Naftalin RJ (2008b) Osmotic water transport with glucose in GLUT2 and SGLT. Biophys J 94:3912–3923

Naftalin R, Arain M (1999) Interactions of sodium pentobarbital with D-glucose and L-sorbose transport in human red cells. Biochim Biophys Acta 1419:78–88

Naftalin RJ, Holman GD (1974) The role of Na as a determinant of the asymmetric permeability of rabbit ileal brush-border to D-galactose. Biochim Biophys Acta 373:453–470

Naftalin RJ, Smith PM, Roselaar SE (1985) Evidence for non-uniform distribution of D-glucose within human red cells during net exit and counterflow. Biochim Biophys Acta 820:235–249

Naftalin RJ, Green N, Cunningham P (2007) Lactose permease H^+-lactose symporter: mechanical switch or Brownian ratchet? Biophys J 92:3474–3491

Nelson PJ, Rudnick G (1979) Coupling between platelet 5-hydroxytryptamine and potassium transport. J Biol Chem 254:10084–10089

Nguitragool W, Miller C (2007) Inaugural article. CLC Cl/H^+ transporters constrained by covalent cross-linking. Proc Natl Acad Sci USA 104:20659–20665

Olkhova E, Hunte C, Screpanti E, Padan E, Michel H (2006) Multiconformation continuum electrostatics analysis of the NhaA Na^+/H^+ antiporter of *Escherichia coli* with functional implications 1. Proc Natl Acad Sci USA 103:2629–2634

Onsager L (1931a) Reciprocal relations in irreversible processes. I. Phys Rev 37:405–426

Onsager L (1931b) Reciprocal relations in irreversible processes. II. Phys Rev 38:2265–2279

Panayotova-Heiermann M, Loo DD, Wright EM (1995) Kinetics of steady-state currents and charge movements associated with the rat Na^+/glucose cotransporter. J Biol Chem 270:27099–27105

Patlak CS, Goldstein DA, Hoffman JF (1963) The flow of solute and solvent across a two-membrane system. J Theor Biol 5:426–442

Peusner L (1986) Hierarchies of energy-conversion processes. 3. Why are Onsager equations reciprocal—the Euclidean geometry of fluctuation—dissipation space. J Theor Biol 122:125–155

Pifl C, Singer E (1999) Ion dependence of carrier-mediated release in dopamine or norepinephrine transporter–transfected cells questions the hypothesis of facilitated exchange diffusion. Mol Pharmacol 56:1047–1054

Prausnitz JM, Lichtenthaler RN, Azevedo EGD (1986) Molecular thermodynamics of fluid-phase equilibria. Prentice-Hall, Englewood Cliffs, NJ

Prigogine I (1968) Introduction to thermodynamics of irreversible processes. Interscience, New York

Regen DM, Morgan HE (1964) Studies of glucose-transport system in rabbit erythrocyte. Biochim Biophys Acta 79:151–166

Regen DM, Tarpley HL (1974) Anomalous transport kinetics and glucose carrier hypothesis. Biochim Biophys Acta 339:218–233

Reith ME, Xu C, Chen NH (1997) Pharmacology and regulation of the neuronal dopamine transporter. Eur J Pharmacol 324:1–10

Robertson S, Matthies H, Galli A (2009) A closer look at amphetamine-induced reverse transport and trafficking of the dopamine and norepinephrine transporters. Mol Neurobiol 39:73–80

Rudnick G (2006) Serotonin transporters-structure and function. J Membr Biol 213:101–110

Rudnick G, Nelson PJ (1978) Reconstitution of 5-hydroxytryptamine transport from cholate-disrupted platelet plasma membrane vesicles. Biochemistry 17:5300–5303

Saint-Martin P, Lespinat PA, Fauque G, Berlier Y, Legall J, Moura I, Teixeira M, Xavier AV, Moura JJ (1988) Hydrogen production and deuterium–proton exchange reactions catalyzed by desulfovibrio nickel(II)-substituted rubredoxins. Proc Natl Acad Sci USA 85:9378–9380

Saunders C, Ferrer JV, Shi L, Chen J, Merrill G, Lamb ME, Leeb-Lundberg LM, Carvelli L, Javitch JA, Galli A (2000) Amphetamine-induced loss of human dopamine transporter activity: an internalization-dependent and cocaine-sensitive mechanism. Proc Natl Acad Sci USA 97:6850–6855

Schwartz JW, Blakely RD, DeFelice LJ (2003) Binding and transport in norepinephrine transporters. Real-time, spatially resolved analysis in single cells using a fluorescent substrate. J Biol Chem 278:9768–9777

Schwartz JW, Novarino G, Piston DW, DeFelice LJ (2005) Substrate binding stoichiometry and kinetics of the norepinephrine transporter. J Biol Chem 280:19177–19184

Semenza G, Kessler M, Hosang M, Weber J, Schmidt U (1984) Biochemistry of the Na^+, D-glucose cotransporter of the small-intestinal brush-border membrane. The state of the art in 1984. Biochim Biophys Acta 779:343–379

Semenza G, Kessler M, Schmidt U, Venter JC, Fraser CM (1985) The small-intestinal sodium-glucose cotransporter(s) 1. Ann NY Acad Sci 456:83–96

Singh SK, Yamashita A, Gouaux E (2007) Antidepressant binding site in a bacterial homologue of neurotransmitter transporters. Nature 448:952–956

Singh SK, Piscitelli CL, Yamashita A, Gouaux E (2008) A competitive inhibitor traps LeuT in an open-to-out conformation 1. Science 322:1655–1661

Sitte HH, Hiptmair B, Zwach J, Pifl C, Singer EA, Scholze P (2001) Quantitative analysis of inward and outward transport rates in cells stably expressing the cloned human serotonin transporter: inconsistencies with the hypothesis of facilitated exchange diffusion. Mol Pharmacol 59:1129–1137

Smirnova I, Kasho V, Choe JY, Altenbach C, Hubbell WL, Kaback HR (2007) Sugar binding induces an outward facing conformation of LacY 1. Proc Natl Acad Sci USA 104:16504–16509

Stein WD (1989) Kinetics of transport: analyzing, testing, and characterizing models using kinetic approaches. Methods Enzymol 171:23–62

Sulzer D, Sonders MS, Poulsen NW, Galli A (2005) Mechanisms of neurotransmitter release by amphetamines: a review. Prog Neurobiol 75:406–433

Supplisson S, Roux MJ (2002) Why glycine transporters have different stoichiometries. FEBS Lett 529:93–101

Tolman RC (1925) The principle of microscopic reversibility. Proc Natl Acad Sci USA 11:436–439

Turner RJ (1981) Kinetic analysis of a family of cotransport models. Biochim Biophys Acta 649:269–280

Ussing HH (1949) The active ion transport through the isolated frog skin in the light of tracer studies. Acta Physiol Scand 17:1–37

Van Camp B, Crow R, Peng Y, Varela M (2007) Amino acids that confer transport of raffinose and maltose sugars in the raffinose permease (RafB) of *Escherichia coli* as implicated by spontaneous mutations at Val-35, Ser-138, Ser-139, Gly-389 and Ile-391. J Membr Biol 220:87–95

Walden M, Accardi A, Wu F, Xu C, Williams C, Miller C (2007) Uncoupling and turnover in a Cl^-/H^+ exchange transporter. J Gen Physiol 129:317–329

Wegscheider R (1901) Simultaneous equations and the relationships between thermodynamic and reaction kinetic homogeneous system. Z Phys Chem Stoch Verwand E 39:257–303

Weyand S, Shimamura T, Yajima S, Suzuki S, Mirza O, Krusong K, Carpenter EP, Rutherford NG, Hadden JM, O'Reilly J, Ma P, Saidijam M, Patching SG, Hope RJ, Norbertczak HT, Roach PC, Iwata S, Henderson PJ, Cameron AD (2008) Structure and molecular mechanism of a nucleobase-cation-symport-1 family transporter. Science 322:709–713

Whitesell RR, Regen DM, Beth AH, Pelletier DK, Abumrad NA (1989) Activation energy of the slowest step in the glucose carrier cycle: break at 23 degrees C and correlation with membrane lipid fluidity. Biochemistry 28:5618–5625

Wilbrandt W, Rosenberg T (1961) The concept of carrier transport and its corollaries in pharmacology. Pharmacol Rev 13:109–183

Zerangue N, Kavanaugh MP (1996) Flux coupling in a neuronal glutamate transporter. Nature 383:634–637

Zeuthen T, Zeuthen E (2007) The mechanism of water transport in Na^+-coupled glucose transporters expressed in *Xenopus* oocytes. Biophys J 93:1413–1416

Zeuthen T, Zeuthen E, Macaulay N (2007) Water transport by GLUT2 expressed in *Xenopus laevis* oocytes. J Physiol 579:345–361

Zifarelli G, Pusch M (2009) Conversion of the 2 Cl^-/1 H^+ antiporter ClC-5 in a $NO3^-/H^+$ antiporter by a single point mutation. EMBO J 28:175–182

Zomot E, Bendahan A, Quick M, Zhao Y, Javitch JA, Kanner BI (2007) Mechanism of chloride interaction with neurotransmitter:sodium symporters. Nature 449:726–730